EXPERIMENTAL SIMULATION OF CREVICE CORROSION OF A FUNCTIONALLY GRADED COMPOSITE SYSTEM OF F91 AND FE-12CR-2SI EXPOSED TO HIGH-TEMPERATURE LEAD-BISMUTH EUTECTIC COOLANT

SARA ELIZABETH FERRY

SUBMITTED TO THE DEPARTMENT OF NUCLEAR SCIENCE AND ENGINEERING IN PARTIAL FULFILLMENT OF THE REQUIREMENTS FOR THE DEGREE OF

BACHELOR OF SCIENCE IN NUCLEAR SCIENCE AND ENGINEERING

AT THE

MASSACHUSETTS INSTITUTE OF TECHNOLOGY

June 2011

Signature of Author: _____
Sara Elizabeth Ferry
Department of Nuclear Science and Engineering
May 20, 2011

Certified by: _____
Ronald G. Ballinger
Professor of Nuclear Science and Engineering
Professor of Materials Science and Engineering
Thesis Supervisor

Certified By: _____
Michael P. Short
Postdoctoral Associate
Department of Nuclear Science and Engineering
Thesis Reader

Accepted By: _____
Dennis Whyte
Professor of Nuclear Science and Engineering
Chairman, NSE Committee for Undergraduate Students

EXPERIMENTAL SIMULATION OF CREVICE CORROSION OF A FUNCTIONALLY GRADED COMPOSITE SYSTEM OF F91 AND FE-12CR-2SI EXPOSED TO HIGH-TEMPERATURE LEAD-BISMUTH EUTECTIC COOLANT

By

Sara Elizabeth Ferry

ABSTRACT

In a system in which metal corrosion is of concern to its long-term structural integrity, crevice corrosion can be a significant cause of damage. Small crevices in a metal exposed to a working fluid (such as a reactor's coolant) may be prone to the development of a localized, aggressive reducing environment. If the metal relies on a passivating layer of oxides for corrosion protection, it may be vulnerable to corrosion attack within the crevice due to a drastically reduced oxygen potential and low pH. Furthermore, in a liquid metal environment, the reducing conditions combined with typically high solubilities of alloy components in the liquid metal can result in severe, localized crevice corrosion that surpasses that which might occur in the aqueous environment of a LWR. In this study, F91 and Fe-12Cr-2Si, two alloys used in previous experiments were exposed to lead-bismuth eutectic maintained at 715°C with a cover gas of pure hydrogen for thirty hours. The conditions were kept extremely reducing, via the initial removal of oxygen and the subsequent maintenance of an environment of pure hydrogen gas, in order to simulate conditions inside a crevice. Following the experiment, the materials were analyzed for corrosion damage via optical microscopy, scanning electron microscopy, and energy-dispersive x-ray spectroscopy. F91 was found to have sustained significant corrosion damage, as expected based on previous experiments, in addition to chromium depletion at the sample surface. Fe-12Cr-2Si was also found to have sustained corrosion damage as a result of lead-bismuth attack. No significant oxide formation or alloying element depletion was observed at the Fe-12Cr-2Si surface. The observed damage in Fe-12Cr-2Si was not entirely expected due to its excellent corrosion resistance in less reducing environments. This raises the concern that crevice corrosion could be an important damage mechanism in applications of the Fe-12Cr-2Si/F91 composite if crevices are present, either due to design flaws or due to cracking during service.

Thesis Supervisor: Ronald G. Ballinger
Professor of Nuclear Science and Engineering
Professor of Materials Science and Engineering

TABLE OF CONTENTS

For Lily and Luca

1. Introduction

Lead-bismuth eutectic (LBE) has been identified as a possible coolant for future reactors by the U.S. DOE Generation IV reactor program, which intends to use novel coolants and reactor designs in order to improve reactor efficiency, safety, and cost ??. LBE has many attractive properties as a potential coolant for a fast reactor: it has a very high heat capacity, is not reactive with air (as opposed to liquid sodium), and is self-shielding from gamma radiation [2]. However, it is highly corrosive to most structural metals via liquid metal attack and dissolved oxygen transport [3, 5]. This renders the feasibility of such a reactor's successful operation questionable.

Previous work led to the development of a functionally graded composite material system designed to resist LBE corrosion, consisting of a structural layer of F91 weld overlaid with a highly corrosion-resistant Fe-12Cr-2Si layer. The composite was developed specifically for use in reactor environments in which lead or LBE is the working fluid [3]. The corrosion resistance of each alloy was tested in a variety of oxygen potentials, temperatures, and exposure durations. However, crevice corrosion had not yet been considered. Crevice corrosion can be an important damage mechanism in metals. Depletion of oxygen inside the crevice can lead to a significantly reduced ability to form a passivating oxide layer that protects against further corrosion, leading to significant localized corrosion damage inside the crevice [4].

In order to simulate crevice corrosion, the experimental setup from previous exposure tests was adapted to simulate the highly reducing environment inside a crevice. Of particular interest was the behavior of the Fe-12Cr-2Si, whose primary function is to provide the majority of the corrosion resistance for the composite. The adaptation of the experimental setup, and the results of the exposure test, form the basis of this thesis.

The key results for an exposure time of 30 hours at 715 °C are as follows:

- Alloy F91, the structural layer of the composite, sustained significant corrosion damage under these conditions. Chromium was observed to be depleted at the metal surface, further diminishing the ability of the F91 to form a protective scale. This agrees with previous tests, which showed F91 to be highly vulnerable to LBE attack.
- Fe-12Cr-2Si, the protective layer of the composite, also sustained corrosion damage via LBE attack, although to a lesser extent than the F91. This conclusion is significant because Fe-12Cr-2Si had not been found to sustain corrosion damage in previous experiments.

2. Background

2.1. **Results Summary from the Primary Experiment.** This project is an extension of the doctoral projects of Michael Short and J. Y. Lim. It was carried out in the H. H. Uhlig Corrosion Laboratory at the Massachusetts Institute of Technology, within the Department of Nuclear Science and Engineering.

The research was focused on the corrosion of structural materials in LBE cooled reactors. Corrosion is a significant issue in these reactors, thus the overarching goals of these experiments were to (1) identify a material(s) that display excellent corrosion resistance to LBE under conditions representative of the environment inside an operating LBE-cooled reactor and (2) show that the material can be economically produced and manufactured on an industrial scale.

2.1.1. *The Composite Metal Approach, and Alloy Selection.* A structural material used in the fuel cladding and coolant piping of an LBE cooled fast reactor must meet the following requirements.

- Long term retention of structural integrity under operating conditions for the reactor lifetime

- Low cost of production
- Excellent corrosion resistance during LBE exposure at reactor operating temperatures

In a review of available alloys and materials, no single material was found to be able to meet all of these conditions [3]. Therefore, a composite approach was taken: a high-strength steel would be weld-overlaid with an alloy that possesses superior corrosion resistance properties.

F91[1] was chosen as the structural layer. The quenched and tempered bainitic/martensitic microstructure in conjunction with the presence of M_xC_y carbides and $M_xN_yC_z$ carbonitrides dispersed throughout the metal lattice increase the alloy's strength by impeding dislocation movement, and consequently reducing creep rates. F91 displays eetxcellent radiation damage resistance, creep resistance, exhibits ductile behavior over a wide range of temperatures, and has a high Charpy impact energy [6]. Cladding or coolant piping made primarily from F91 would thus be able to stand up to the aggressive mechanical and thermal conditions inside an LBE-cooled fast reactor.

F91 is weld overlaid with a Fe-Cr-Si alloy. The similarities in composition, in conjunction with the weld overlay process, would ensure excellent microstructural mixing and ensure the durability of the composite interface [3].

Chromium and silicon were ideal alloying components for the corrosion resistant layer. They have a tendency to form passivating oxides that are stable at low oxygen potentials, such as Cr_2O_3, SiO_2, $Fe(Fe_xCr_{2x})O_4$, and $Fe(Fe_xSi_{2x})O_4$.[3] Together, their effect is synergistic: adding silicon in the right amounts to a steel alloyed with chromium can result in a dramatic increase in the ability of the alloy to form protective passive oxide layers [7]. These layers will form quickly even at low oxygen concentrations. Cr_2O_3 forms a dense, nonporous layer that is highly protective against liquid metal attack; a network of SiO_2

[1] F91 is a steel alloy with between 8 and 12 % Cr content, in addition to about 1% Mo and small (less than 1%) amounts of Si, V, and Ni.

and $Fe(Cr,Si_2)O_4$ precipitates forms beneath this layer and imparts additional corrosion resistance [8]. While aluminum provides excellent corrosion protection as well, it was excluded from the development of this alloy because of its poor weldability [3, 12]. Fe-Cr-Al alloys can be susceptible to hot cracking when welded, and since a key requirement of the composite is its ability to be easily fabricated into piping and cladding, it was not selected for study.

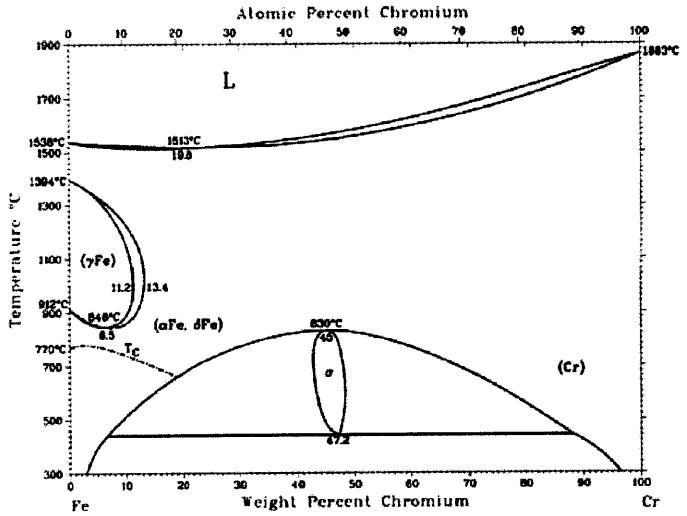

FIGURE 1. The phase diagram shows the solubility of Cr in Fe. At reactor operating temperatures of between 600 and 700°C, it is crucial that Cr does not precipitate into σ-Cr [9].

It is important to select the optimum concentrations of Cr and Si. Enough Cr and Si must be present in the Fe-Cr-Si alloy in order to ensure that sufficiently dense oxide layers will form [8, 3]. However, too much chromium will lead to the formation of σ-Cr precipitates [9], whose solubility in iron is shown in Figure 1. These precipitates weaken the material by increasing the likelihood of brittle fracture and crack propagation along the grain boundaries where these precipitates are present [10, 11]. Similarly, the presence of too much silicon also leads to deleterious effects, via embrittlement of the alloy, in

Sample	Fe	Cr	Si	W	Mo	Cu
F91	88.0147	9.4351	0.3478	0.0717	0.9606	0.1388
Fe-12Cr-2Si	84.6493	13.1086	1.9975	0.1736	0.0006	0.0002

Sample	Ni	Mn	V	S	P	Al
F91	0.2797	0.5088	0.1918	0.0243	0.0173	0.0094
Fe-12Cr-2Si	0.0058	0.0190	0.0004	0.0029	0.0005	0.0416

Sample	Pb	Bi	As	Fe	Sb	Sn	Cu	Ni	Cr
Lead	95.9336	4.0661	0	0.0003	0	0	0	0	—
Bismuth	0	99.9974	0	0	0	—	0	—	0.0026

FIGURE 2. The table shows the compositions of the actual F91 samples, Fe-12Cr-2Si samples, Pb, and Bi used in this study, as verified by ICP-MS [3].

particular due to radiation-induced segregation of alloying elements at grain boundaries during reactor operation [13, 14]. (The solubility of silicon in iron is shown in Figure 5 for further reference. Based on these considerations, a final composition of Fe-12Cr-2Si was selected [3]. The Fe-12Cr-2Si alloy protects the F91 from coming into contact with the LBE, and the Fe-12Cr-2Si itself is protected from LBE attack by the passivating layers that form on its surface [17]. Figure 2 shows the compositions of the actual F91 samples, Fe-12Cr-2Si samples, Pb, and Bi used in this study, as verified by IC-PMS (Inductively Coupled Plasma Mass Spectroscopy) [3].

2.1.2. *Summary of previous work in the Fe-Cr-Si system.* The experiments for this project spanned several years, and so a brief summary is presented here for background purposes. Dr. Michael Short's Ph.D thesis, *The Design of a Functionally Graded Composite for Service in a High Temperature Lead and Lead-Bismuth Cooled Nuclear Reactor* (see Reference [3]) is highly recommended for an in-depth explanation of the studies performed to validate the corrosion resistance and structural integrity of this composite.

Note that Fe-12Cr-2Si is a new alloy, and was custom-made at Special Metals, Inc. in West Virginia for this project.

- Static corrosion testing of F91 and Fe-12Cr-2Si was performed via an experimental procedure similar to the one described in Section 3.4 of this thesis. Both materials were exposed to LBE from 600 to 715°C in reducing and oxidizing environments with respect to the formation of iron oxides. It was found that F91 corroded severely, as expected, while Fe-12Cr-2Si performed very well in both oxidizing and reducing environments and displayed very little corrosion damage: chromium and silicon oxides form at much lower oxygen potentials than do lead and bismuth oxides, as can be seen from the Ellingham diagram in Figure 3. Figure 6 and Figure 7 show micrographs of F91 and Fe-12Cr-2Si following exposure to LBE in both environments after 506 hours. It is evident from the figures that F91 was highly vulnerable to attack, while Fe-12Cr-2Si was essentially unaffected.
- In order to show that the FGC was commercially viable, it was produced on a commercial scale using domestic vendors. Fe-12Cr-2Si weld wire was overlaid onto specially machined extrusion billets of F91 in a process known as gas tungsten arc welding, which is shown in Figure 8. F91 overlaid with the protective Fe-12Cr-2Si on its inner diameter can be drawn into piping; F91 overlaid with Fe-12Cr-2Si on its outer diameter can be drawn into smaller diameter tubing for fuel cladding. The completed welds have been undergoing testing to show that the completed projects are indeed viable structural materials for an LBE cooled fast reactor, with very positive results thus far. Figure 4 displays the microstructure of the as-welded Fe-12Cr-2Si/F91 interface and illustrates the microstructural mixing at the interface between Fe-12Cr-2Si and F91 on an ID-clad billet (intended for extrusion into coolant piping).
- Diffusion couples of Fe-12Cr-2Si and F91 were sealed in quartz ampoules and aged at high temperature for varying amounts of time. Hardness testing was then performed across the interface to examine how the hardness profile changed with time.

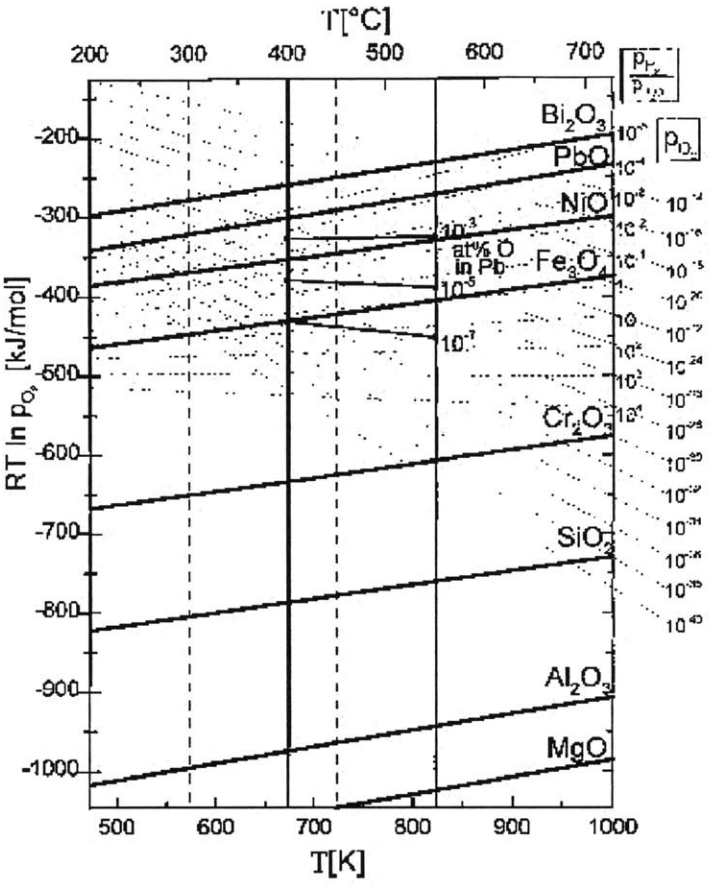

FIGURE 3. Chromium and silicon oxides are stable at much lower oxygen potentials than lead and bismuth oxides. In the LBE environment, this means that protective chromium and silicon oxides quickly form on the Fe-12Cr-2Si as long as a certain temperature-dependent oxygen potential characterizes the system [18].

The purpose of this testing was to show that silicon diffusion from the Fe-12Cr-2Si into the F91 over time would not be so severe that the Fe-12Cr-2Si was significantly depleted in silicon, which would lead to a reduced ability to self-passivate. The most important application to consider is that of fuel cladding, since the cladding walls

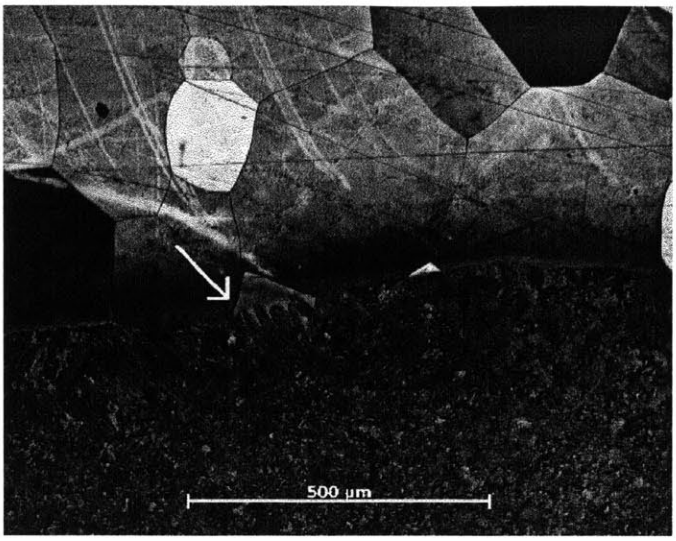

FIGURE 4. ID-clad billet extrusion: Fe-12Cr-2Si (top, large grained, ferritic alloy) has been weld overlaid on F91. The arrow points to an area of microstructural mixing between the ferritic Fe-12Cr-2Si and the martensitic F91. The mixing layer is very thin, but it ensures that the bond between the two materials is strong [3].

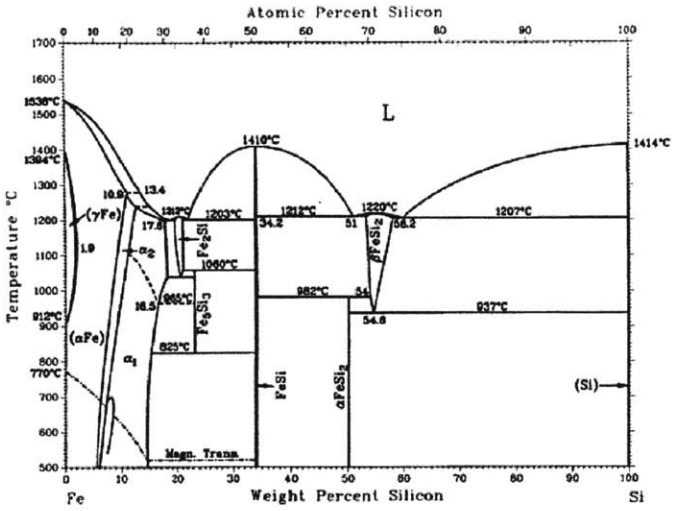

FIGURE 5. The binary phase diagram for silicon and iron shows the solubility of Si, allowing for effective determination of weight percents of Si in the corrosion resistant layer [9].

are typically very thin: the Fe-12Cr-2Si must be thick enough that surface concentrations of silicon are not depleted. Again, results were highly encouraging, and are shown graphically in Figure 9.

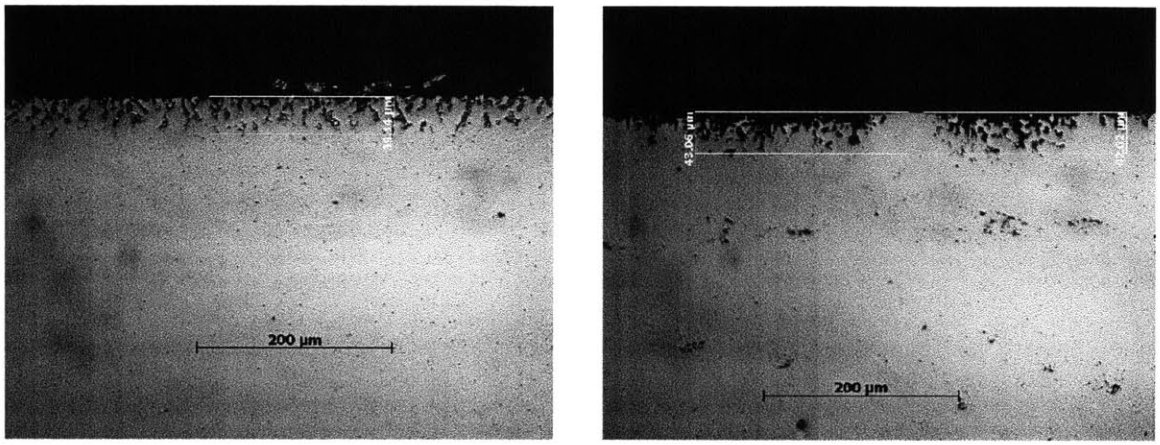

FIGURE 6. F91 samples exposed to LBE for 506 hours in a reducing (left photograph) and oxidizing (right photograph) environment at 715 and 700°C respectively. The experimental procedures were the same as those used in this thesis, and are detailed in subsequent sections. Significant corrosion damage has occured, with attack channels that are approximately 40 μm deep. LBE residue is evident in attack channels for the reducing-environment sample; metal adheres to metal, so this indicates that there was little-to-no oxide formation on the sample [3].

2.2. **Crevice Corrosion.** Crevice corrosion is of particular significance to self-passivating materials like Fe-12Cr-2Si. These alloys gain their corrosion resistance from their tendency to form passive surface films that protect the underlying metal from attack [19]. For a metal in contact with a fluid, if a crevice or other occluded region is present at the surface, the fluid in the crevice may become extremely depleted in oxygen, thus preventing the metal from forming a passivating oxide layer in the localized region inside the crevice [19]. Without the passivating oxide layer, the exposed metal can be vulnerable to corrosion attack. This is especially true when the metal exhibits significant solubility within the liquid metal. Figure

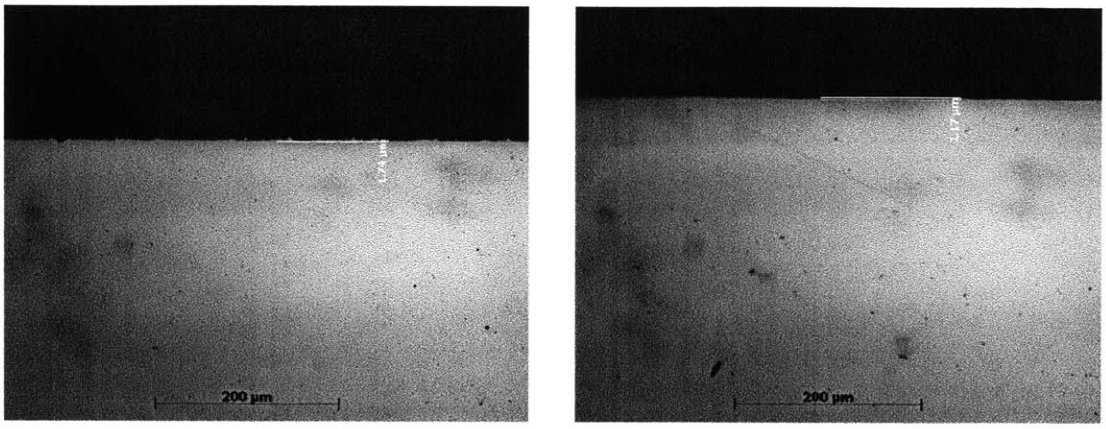

FIGURE 7. Fe-12Cr-2Si exposed to LBE for 506 hours. Samples were exposed to LBE in a reducing (left photograph) and oxidizing (right photograph) environment at 715 and 700°C respectively. The Fe-12Cr-2Si is highly resistant to corrosion, even in the reducing environment, in which there is minimal oxygen available to form protective oxide layers [3].

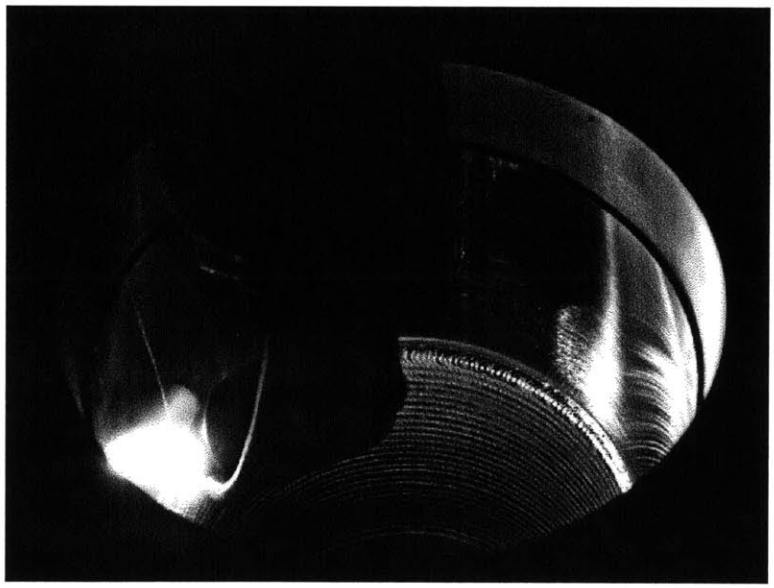

FIGURE 8. Fe-12Cr-2Si being weld overlaid onto the inner diameter of F91 by gas tungsten arc welding (GTAW) [3].

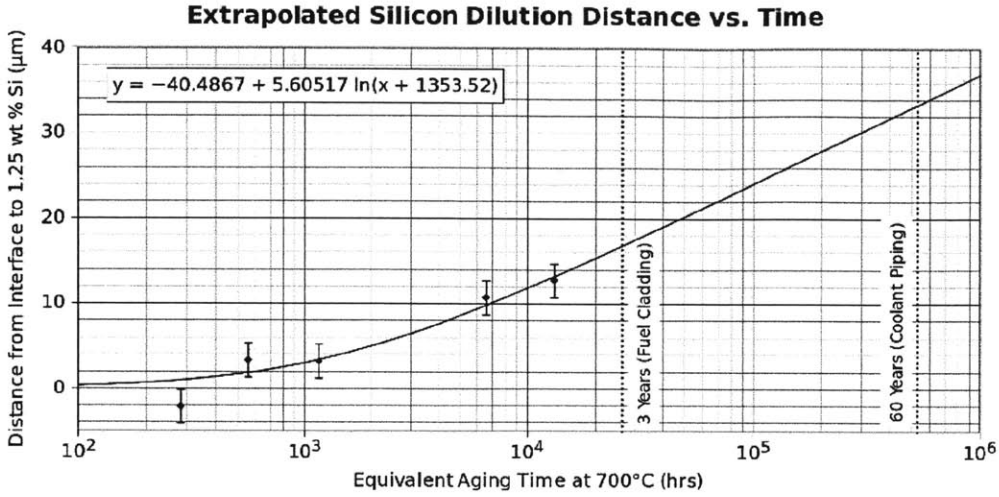

FIGURE 9. Curve showing extrapolated silicon dilution distances in the FGC. The expected lifetime of fuel cladding is three years. At this point, expected silicon dilution distance is approximately 17 μm [3].

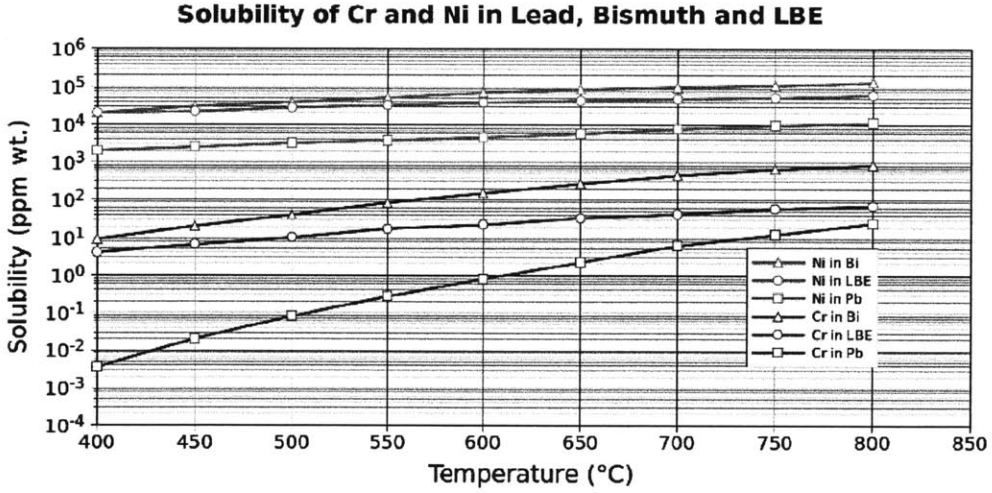

FIGURE 10. Cr and Ni solubilities in liquid LBE. Nickel's high solubility eliminates it from consideration as an alloying element in structural steels for LBE environments [3, 8].

10 shows the solubility of two common alloying elements, chromium and nickel, in liquid LBE. Nickel exhibits very high solubility, eliminating it as an alloy addition in an LBE-cooled system.

Inside the crevice, there is significantly less mass transport occurring due to its isolation from the bulk fluid. The oxygen inside the crevice is quickly used up as the passivating metal forms oxides. The oxygen is not replaced, and so its concentration inside the crevice quickly drops. In particular, the oxygen potential can drop below the oxygen potentials required for chromium and silicon oxide formations [4]. Damage occurs when passivating layers are not able to form inside the crevice at all, or when they are breached or break away, and are not able to reform due to drastically reduced oxygen potentials [20].

In a practical application, the damage caused by crevice corrosion is largely determined by the geometry of the defect in question, namely, the width, depth, and shape of the crevice [21]. If the crevice is shallow enough, crevice corrosion may not occur because the difference in mass transport internal and external to the defect may not be significant enough to result in the extreme oxygen depletion that is characteristic of severe crevice corrosion. Beyond a certain critical crevice depth, however, corrosion damage can be significant throughout the localized area of the crevice [4]. Chromium is an alloying element that can be highly effective in minimizing the corrosion damage within crevices due to its ability to form passivation layers even in very low oxygen potentials [4]. However, because the environment inside a crevice can become so severely depleted in oxygen, even alloys containing chromium can be susceptible to crevice corrosion. This particular corrosion mechanism is also characterized by a high rate of damage; for ferritic steels like Fe-12Cr-2Si, the damage is generally most severe near the end of the crevice [22, 23].

Crevice corrosion begins after the passivating oxides that have begun to form on a surface break down, although the breakdown mechanism is not entirely understood [4].

The best method of prevention against crevice corrosion is to ensure that crevices are not formed during the fabrication of structural components [24]. For the case in which a material is exposed to liquid metal that can dissolve the alloying elements, it is possible to limit the damage through the use of elements that have limited solubility in the liquid. As Figure 5 shows, silicon has very limited solubility in LBE. Thus, it is likely that a silicon rich layer will develop on the surface due to selective dissolution of the other alloying elements. It was hoped that the silicon rich layer, if it formed, would at least slow further dissolution in extremely reducing environments.

3. Materials and Experimental Methods

3.1. Obtaining the materials. The F91 was initially procured from Metalmen Sales, Inc. in New York. The Fe-12Cr-2Si was initially procured as a custom-made alloy. When the composite piping was produced in a steelworks setting, a forged billet of Fe-12Cr-2Si was drawn into weld wire for creating the weld-overlay of the protective alloy on the extruded T91 pipes[2]. This billet would later provide additional Fe-12Cr-2Si samples for experimentation.

The lead and bismuth were ordered from Surepure Chemicals, Inc. in Florham Park, New Jersey. The purity of each metal was guaranteed to 99.999%. They arrived in 34 kg (75 lb) buckets of granular lead and needle-shaped bismuth. This allowed for precise mixing of specific amounts of lead and bismuth when preparing the eutectic alloy for the exposure tests.

[2]After extrusion into tubing, F91 is frequently referred to as T91. The unextruded alloy is always referred to as F91.

3.2. Preparing the materials for exposure.

3.2.1. *F91 and Fe-12Cr-2Si samples.* Figure 11 shows two samples used in one of the LBE exposure experiments. The larger sample is F91; the smaller sample is Fe-12Cr-2Si. (Note that these samples were photographed post-exposure during a problematic test: the thick black oxides that developed on them were indicative of oxygen contamination.)

FIGURE 11. An exposed sample of F91 (bottom) is shown with an exposed sample of Fe-12Cr-2Si post-exposure. A thick, black oxide film has developed on their surfaces due to oxygen contamination during the experiment.

The F91 sample was 30 mm long; the Fe-12Cr-2Si sample was 20 mm long. Two holes[3] were drilled in the top center of each sample using a 1.27 mm drill and drill press to facilitate attachment to the sample holder used during the exposure tests.

Once cut and drilled, the samples were attached using CrystalBond to a metal platen of a Buehler EcoMet 3000 polisher with an AutoMet 2 automatic polishing head. The CrystalBond ensured secure attachment of the samples to the plate without requiring further drilling or mounting, and also allowed for easy, non-destructive removal of the samples once the polishing was complete.

After the samples were attached to the plate, it was attached to the polishing head of the EcoMet polisher. The samples were first ground flat using 120 grit SiC Carbimet sandpaper, so that subsequent polishing steps would affect each sample equally. The samples were then polished using SiC Carbimet sandpapers of 180, 240, 600, 800, and 1200 grit. Each polishing step was continued until the surface of interest on each sample had achieved identical finishes (on average, this took between three and five minutes, assuming that the polished surfaces of each sample on the plate were on the same plane.) Subsequent to the sandpaper polishing steps, MetaDipolycrystalline diamond suspensions of 6 μm, 3 μm, and 1 μm were used to further refine the polishing process. Each diamond suspension polishing step lasted for approximately two minutes. When a suitable finish had been achieved using the 1 μm diamond suspension, a final polish was carried out using MasterPrep 50 nm alumina suspension for two more minutes. A force of between four and five pounds per sample was used throughout the entirety of the sample polishing process, with a polisher platen rotational speed of 150-170 rpm. Polished samples are shown in Figure 12.

[3]Using two pieces of molybdenum wire instead of one to attach the samples to the holder were found to provide better stability for the submerged samples, and ensured that they did not drift upward due to buoyancy in the LBE.

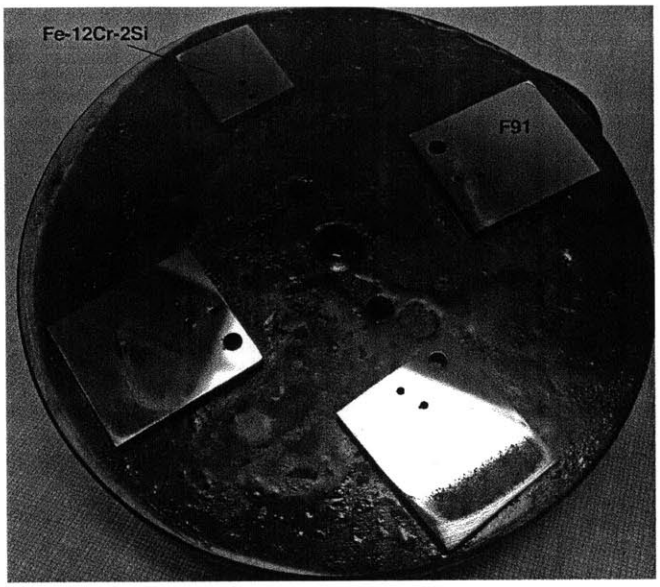

FIGURE 12. Samples of F91 and one of Fe-12Cr-2Si polished in preparation for exposure. Afterwards, they were removed from the plate and cleaned with acetone and ethanol before being attached to the sample holder.

The samples were easily removed from the plate by applying a small amount of force with a flathead screwdriver. They were then sonicated in acetone and ethanol, and wiped with KimWipes and ethanol to clean the polished surfaces of any residue from handling or polishing.

The samples were then attached to a titanium holder used during the exposure experiments with molybdenum wire, which was threaded through each of the two drilled holes to avoid sample flotation in LBE, which is denser than the metals in question. Figure 13 shows the samples being adjusted after initial placement on the sample holder; Figure 14 shows the samples immediately prior to being placed inside the furnace. The molybdenum wire was hooked to prevent the samples from slipping off. During this stage of the experiment setup, it was important to exercise caution that tools or the molybdenum wire did not scratch the polished surface of the samples.

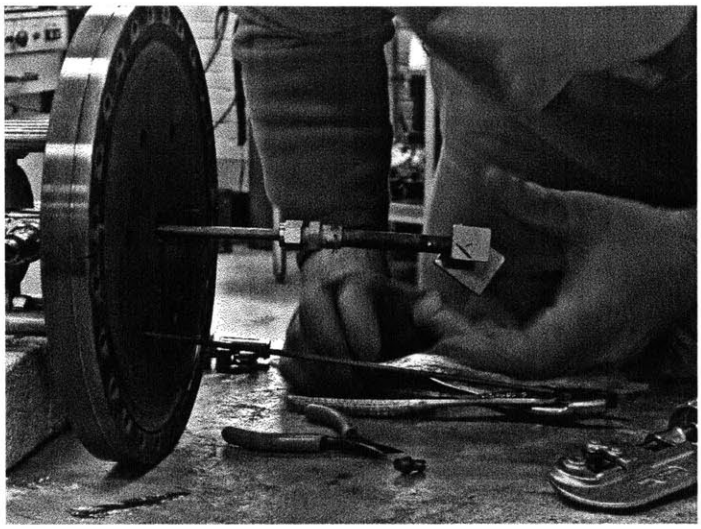

FIGURE 13. The samples being adjusted on the titanium rod. (The polished surface reflects the wood table, giving it a gold appearance in this photograph.) Note that the titanium rod was attached to the furnace lid with the same molybdenum wire, which was an ideal attachment wire in this experiment due to its strength, flexibility, and temperature resistance. The entire holder can be moved up and down. Also note the in-furnace thermocouple, which protrudes beneath the samples.

3.2.2. *Preparing the Lead-Bismuth Eutectic and the Fe, Cr test pieces.* 392.45 g of solid bismuth pellets and 318.5 g of solid lead pellets were combined to form the eutectic mixture (55.2 % Bi, 44.8 % Pb).

The solid lead and bismuth mixture was placed inside a McDanel Advanced Ceramic ACN3768 alumina crucible. The crucible was placed on top of an alumina plate. Test pieces of pure iron and chromium were placed on the alumina plate alongside the crucible. These test pieces, prior to the test, were completely unoxidized. By examining them before and after the test, it was possible to have a qualitative measurement of whether oxygen had entered into the system from outside, and to confirm that reducing conditions were preserved during the test. (The test pieces are particularly useful in this experiment, because the environment is

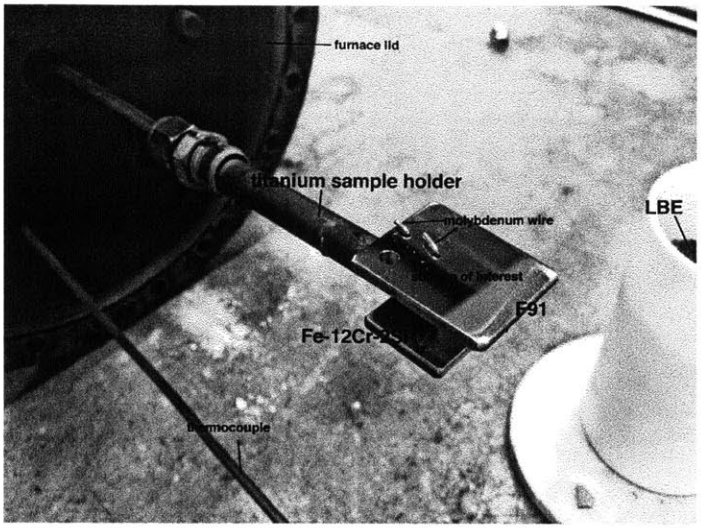

FIGURE 14. The samples have been securely attached to the titanium holder using molybdenum wire, which has been carefully clipped and bent to secure the samples. The polished surface of the samples faces outwards. Note the crucible of prepared LBE alloy in the foreground.

intended to be kept as reducing as possible, with an absolute minimum of oxygen content). The crucible with the Pb-Bi mixture and the test pieces on the plate are shown in Figure 15.

3.3. Preparing the test set up: the furnace/autoclave system. Once the materials were prepared, experimental set up began. The alumina crucible and plate were placed in the center of a stainless steel autoclave which was held inside an upright Mellen cylindrical furnace. The experimental setup contained two furnaces, so that oxidizing and reducing environments could be tested simultaneously: this portion of the experiment utilized only one furnace. The temperature inside the test chamber was monitored with Honeywell K-Type thermocouples. Gas inflow to the furnace was controlled and monitored via a custom built gas mixing system.

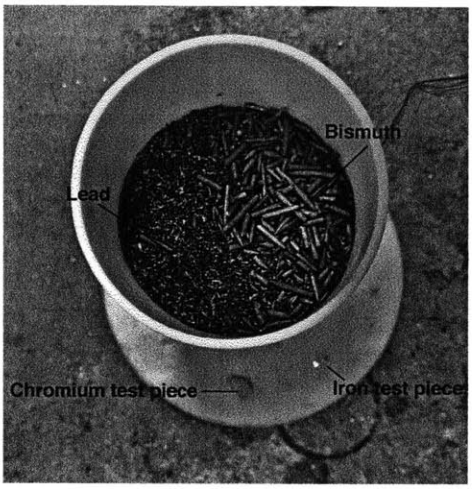

FIGURE 15. The lead and the bismuth, prior to melting, inside the alumina crucible. The bismuth, visible toward the right in this picture, has a needle-like structure in the granular form as-ordered. The iron and chromium test pieces are visible on the alumina plate: the iron test piece is on the left, and the smaller iron pieces are on the right.

A copper gasket seal, matched to the furnace opening's diameter, was fitted before placing the furnace lid with attached samples on top of it. The gasket ensured an air tight seal (see Figure 16). The furnace lid was then bolted down, using Jet-Lube 550 Petrochemical Grade Anti-Seize Lubricant to provide a barrier between the metal furnace lid and the bolts.[4] There were 24 bolts in total: they were secured down in opposing pairs, to ensure an even distribution of pressure on the gasket. Following this screw-to-opposite-screw pattern, the screws were torqued down with 100, 130, and 160 lb of force. (The 160 lb torque was applied twice.)[5] The gas piping was then connected to the furnace with Swagelok fittings. The secured lid is shown in Figure 17. The samples could be moved up and down, and held in place; initially, the samples were held in the 'up' position, so that they were

[4]The lubricant ensured that the bolts would be able to be removed easily after the furnace has been soaking at high temperature during the course of the experiment.

[5]This seems extraordinarily specific, but it is very important: if the lid is not secured in this way, it is very easy for small leaks to develop between the lid and the copper gasket, allowing oxygen contamination.

not in contact with the lead-bismuth mixture while it is melting, which allowed the exact time that the experiment begins to be determined.

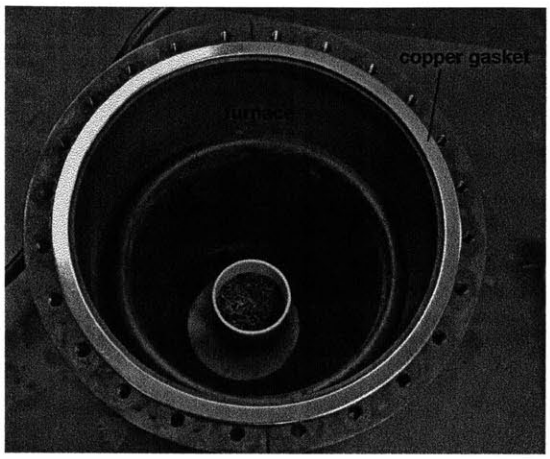

FIGURE 16. The crucible inside the autoclave inside the furnace, with a fresh copper gasket fitted to the furnace opening prior to replacing the lid with the samples.

The gas was controlled and monitored via the setup pictured in Figure 18. Figure 19 shows the overall set up in diagrammatic form.

3.4. **Experimental Procedure: The exposure test.** After screwing down the lid and connecting all thermocouples and tubing, a vacuum (attached to the furnace via a valve fixture, shown in Figure 17) was used to evacuate the test chamber. Pure argon gas, obtained from AirGas, was used to backfill the autoclave and furnace. The furnace was then evacuated with the vacuum once more, and backfilled a second time. This was repeated for a total of three evacuations and backfills. By backfilling with argon gas, it could be ensured that the furnace, once evacuated to vacuum pressure, will not result in an air intake that would contaminate the experimental environment inside the autoclave with oxygen [3]. During the backfill, all of the fittings were also tested for leaks using a soap-water solution at a positive pressure.

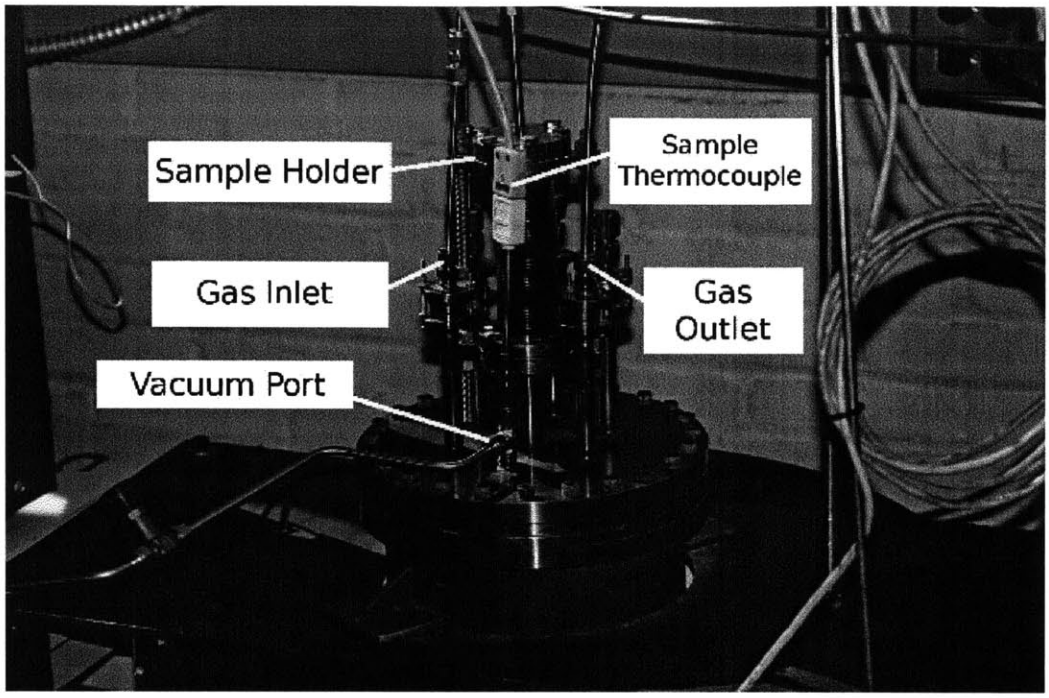

FIGURE 17. The furnace with lid in place [3].

The furnace was cleaned with acetone to remove fingerprints and grease.[6] The furnace was then heated to 400°C to be 'baked out' for approximately six hours before being raised to the testing temperature of 700°C.[7] This allowed the eutectic to fully melt and mix, and it also allowed any oxygen present in the system to burn off. (This oxygen 'burnoff' can be noted in the readings from the moisture

[6]This step is done purely to prevent the unpleasantness that tends to result when fingerprint oil burns off of steel at 700°C.

[7]As a reference to those who may use this setup in the future, note that the reading on the furnace temperature monitor is different from the actual temperature obtained from the in-furnace thermocouples by approximately 110 degrees. As a result, the furnace temperature reading is used to control the setpoint, but the actual temperature data is taken from the thermocouple readout on the computer setup. A typical monitor reading would be upwards of 815°C; the temperature readings on the computer oscillate by ± 1°C around the actual temperature reading. Furthermore, it was found that there is a slight difference of about 15° between the thermocouple in the furnace and the heated lead-bismuth mixture. This result was found by 'sacrificing' a thermocouple to experimental temperature LBE (715°C). Therefore, the computer reading for the furnace thermocouple should be adjusted until it is approximately 15°C *below* the desired temperature for the exposure experiment.

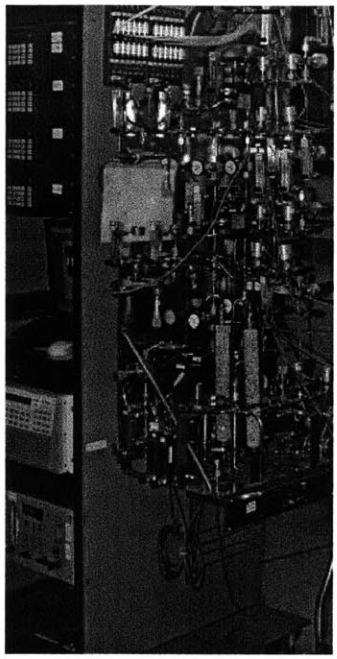

FIGURE 18. This system controls and monitors experimental conditions. Cover gas flows through the sensors and piping on the right, and the monitors and computer system on the left provide continuous feedback regarding moisture levels, temperature, and composition while storing data.

sensors: shortly after the furnace began to reach high temperatures, the moisture levels spiked as combustion of oxygen and hydrogen produced H_2O. It then dropped sharply as all of the available oxygen was burned up.)

The hydrogen gas (also ordered from AirGas) was connected to the experimental setup via stainless steel tubing. When conditions had sufficiently equilibriated[8] and the hydrogen was moving through the system, the samples were lowered into the molten LBE. The exposure lasted for 30 hours. The system was checked regularly and temperature, gas pressure, and moisture levels were monitored between once and twice a day, in addition to constant data recording by computer.

[8]This point was considered to have been reached when the moisture meters zeroed out, implying that all oxygen had been burned out. Previous tests reported that 25-30 hours were required to reach equilibrium [8], so the soak-out at 400°C was left running over night even though moisture levels declined to zero-levels in less time.

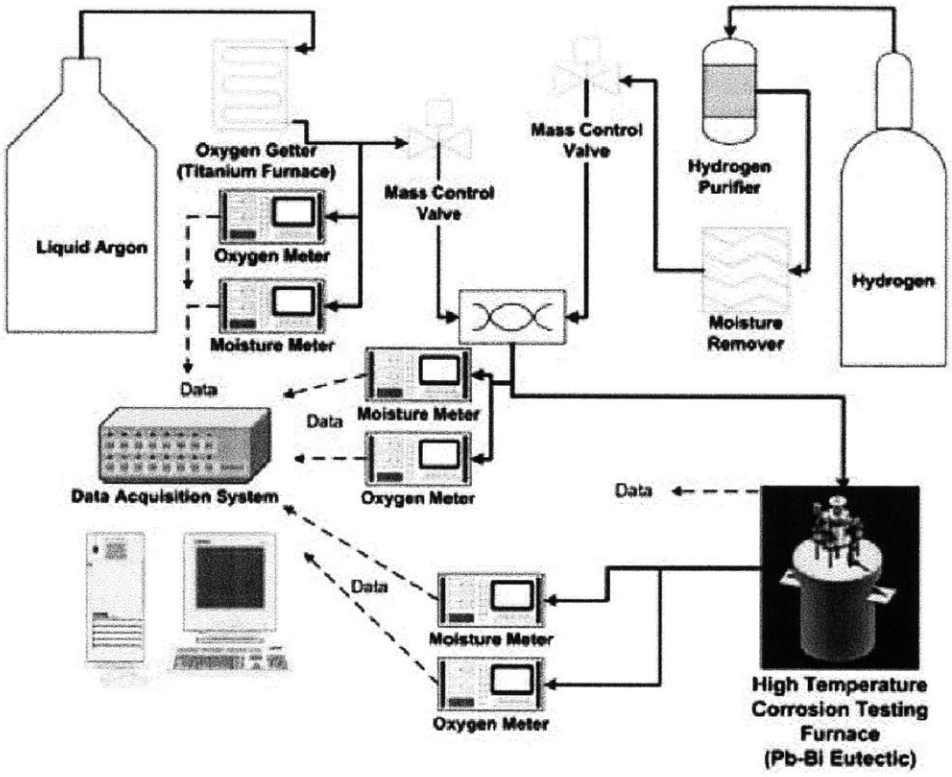

FIGURE 19. A diagram showing the experimental setup [8].

At the end of the test, all valves and gas canisters were closed and the samples were lifted from the eutectic. The furnace was then shut down and allowed to equilibriate to room temperature before the lid was unscrewed and the samples were removed for analysis.

3.5. **Preparing the Exposed Samples for Analysis.** The samples (and the test pieces of Fe and Cr) were photographed immediately after being removed from the furnace. They were then removed from the sample holder (with care being taken not to scratch the samples with the molybdenum wire or with pliers).

A Leco VC-50 low speed diamond saw and an IsoCut wafering blade were used to partition the exposed Fe-12Cr-2Si and F91 into three sections. The first cut was

made across the shorter width dimension. The half of the sample with the drilled holes was put aside; the second half was halved again. The low speed diamond saw allowed for effective cutting of the samples without introducing excessive heat or stress that might affect analysis.

A Struers Prestopress-3 was used to mount the pieces of each sample in Buehler conductive copper mounting mixture. The mounted samples were then polished following the same procedure detailed in Section 3.2.[9] Figure 20 shows the four samples after mounting and polishing.

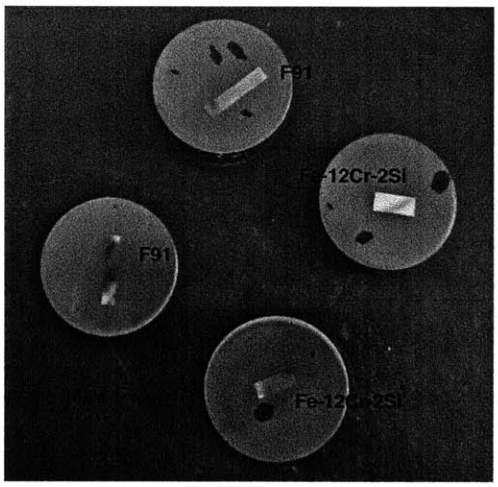

FIGURE 20. The samples, following cutting, mounting, and polishing. The F91 samples are longer than the Fe-12Cr-2Si samples. The exposed face represents a cross-section of the sample, with one of the long edges corresponding to the surface that was polished prior to exposure. This edge was the interface of interest. Note that the black parts of the mounting are simply a result of excess black Bakelite powder from previous mountings being left over inside the press.

3.6. **Optical Microscopy.** The mounted samples were photographed using a Zeiss AxioCam MRc digital camera mounted on a Zeiss metallograph prior to etching.

[9]In this case, a special polishing holder designed for mounted samples was used, rather than attaching the samples to the plate with CrystalBond.

Two results, for 500x magnification of F91 and Fe-12Cr-2Si are shown in Figures 27 and 28 respectively. (Note that the samples were mounted in a Bakelite-copper mixture, thus accounting for the light-colored grains seen floating in the dark mount - in a color photograph, they would look significantly more distinct from the sample metal.)

3.7. **Scanning Electron Microscopy.** Mounted samples of F91 and Fe-12Cr-2Si were lightly coated with gold[10] and examined in a JEOL JSM-5910 scanning electron microscope at a 20 mm working distance and a voltage of 25 kV.

3.8. **EDX analysis.** Using the same SEM facility, energy dispersive x-ray (EDX) maps were acquired for both samples in order to determine (A) if any depletion of alloying elements at the material surface was observable and (B) if lead-bismuth was present in the attack channels. EDX allows the identification of specific elements in a given area of the sample by detecting their characteristic x-rays. EDX mapping allows for the determination of an element's spatial density over the area of interest.

3.9. **Etching and final optical microscopy.** In order to highlight features of interest, F91 was stained for forty seconds with Kaling's reagent, which colors bainite grains more darkly than ferrite grains and highlights carbides. The reagent was prepared with 25 mL of concentrated hydrochloric acid, 25 mL of ethanol, and 0.2 grams of copper chloride ($CuCl_2$). The sample was stained in ten second intervals and immersed in water after each step in order to prevent darker staining than desired.

Fe-12Cr-2Si was engineered to be resistant to corrosion, and so it is was necessary to take a different approach in order to define features of interest on the sample face. 17 mL of 30% hydrogen peroxide (H_2O_2) and 2 mL of water were combined

[10]Because we mounted the samples in copper-infused Bakelite, only a very light coating was used; when the same samples are mounted in black non-conductive Bakelite, it is important to remember to use a thicker gold coating.

in a plastic beaker, to which 1 mL of 50% hydrofluoric acid (HF) was added. Note that plastic labware must be used when working with hydrofluoric acid, which attacks glassware.[11] The sample was etched in ten second intervals for one minute. This etchant attacked grain boundaries and cracks, so it was useful to compare these micrographs with those obtained prior to the etching in order to distinguish corrosion damage from damage induced by the hydrofluoric acid.

All micrographs were taken on the same Zeiss metallograph as before with a mounted Axiocam MRc digital camera.

4. Results: Adapting the Experiment

4.1. **Tests 1 and 2: Lessons Learned.** This is the first time that this experimental setup was used with a pure hydrogen environment. The first two tests were not entirely without problems, as unanticipated drawbacks were faced during the course of the experiments.

The most important limitation to note was the length of time that the hydrogen gas canister lasted. Due to safety regulations, it was not possible to obtain multiple canisters of hydrogen from Airgas (nor was it possible to use a larger canister than the one we used). In previous experiments, hydrogen had been used, but only as a very small fractional part of the gas environment inside the furnaces. It was not anticipated how quickly the hydrogen would be depleted when the cover gas was pure hydrogen. As a result, the hydrogen gas ran out overnight, when it had been expected to last for at least another fifteen hours longer than it did. Therefore, the experiment was already not going to be good for analysis, since we could not know the specific time that the hydrogen ran out. Without hydrogen inside the

[11]Other precautions must also be taken when working with HF as an etchant: full laboratory protection, including wrist guards and a face shield, is advised. Calgonate paste should be easily accessible in the case of skin exposure. Calgonate neutralizes the fluoride ions, which can seep through the skin and stop the heart.

system, air began to seep in, contaminating the LBE and the materials with oxygen. Figures 21 and 22 show the oxide layer that developed on the LBE and the Fe and Cr test pieces during the first test.

FIGURE 21. The LBE after the first test run, during which the hydrogen gas ran out partway through. A thick oxide layer formed on top of the resolidified surface.

The second test was less problematic, but it was evident that some oxygen had still crept into the system. When the samples were removed, a gold patina was visible on the LBE, and the underside of the furnace lid had turned a similar yellowish color (see Figure 23). This is indicative of lead oxide formation: the oxygen contamination was not as severe as in the first test, but was still high enough to invalidate the test.

During the third test, the exposure time was shortened to thirty hours, to ensure that the test would end before the hydrogen ran out or reached a pressure low enough to allow significant air inflow to the system. Either way, it was clear that there were certain difficulties inherent in running pure hydrogen through this

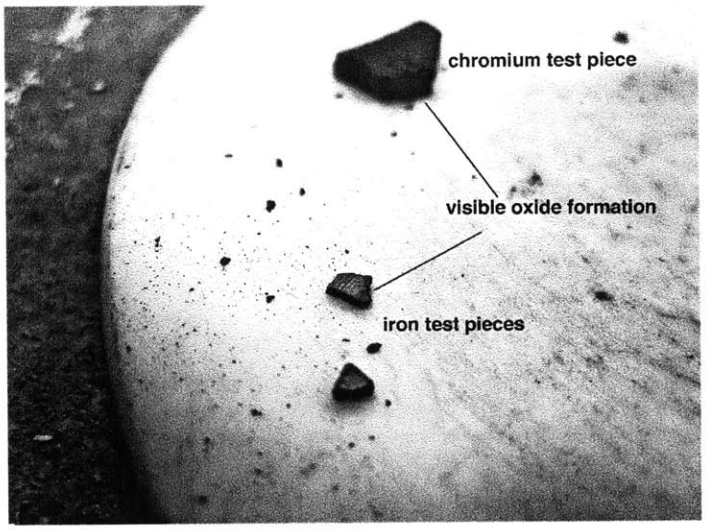

FIGURE 22. The test pieces of Fe (foreground) and Cr (background) after the first test run. A dark oxide layer is visible on both of them, indicating that significant oxygen contamination occurred.

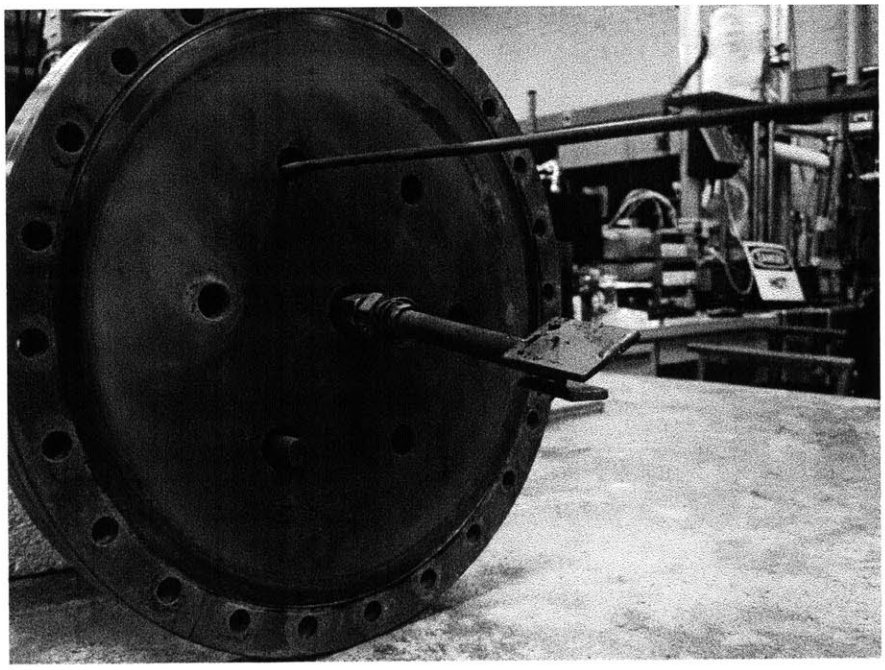

FIGURE 23. The lead vapor film on the underside of the furnace lid has a distinctive yellowish color, indicating lead oxide formation.

particular system: the experimental setup and procedure, as it currently exists, is not conducive to performing exposure tests longer than 30 hours with pure H_2.

4.1.1. *Hydrogen Diffusion.* It is possible to model the hydrogen gas as a static system, since its flow through the system was slow. The system of steel tubing that connects the gas source to the gas mixing system and the furnace considered at room temperature.

For a hydrogen diffusion constant D of 10^{-4} cm^2/s [26] and a 30 hour test, the characteristic diffusion length of hydrogen,

$$2\sqrt{Dt}\ [27]$$

was found to be nearly 6.6 cm. This suggests that hydrogen diffusion out of the experimental setup significantly decreased the time it took for the hydrogen canister to deplete (thus shortening the possible duration of the test). Since a significant length of tubing is used - well over seven hundred inches - and the tube walls are short compared to the characteristic diffusion length (0.035 in, or 0.0841 cm), hydrogen diffusion out of the setup is one possible reason that the hydrogen canister ran out so rapidly.

4.2. **Test Three: Great Success!** The third test run was more successful. The gas valves were closed, the samples removed from the LBE, and the furnace shut off 30 hours after the samples were initially dunked in the LBE. Figure 24 shows the F91 sample following exposure. Figure 25 shows the Fe-12Cr-2Si following exposure. The visibly large grains in the Fe-12Cr-2Si indicate the possibility of preferential corrosion for differently oriented grains: it is possible to distinguish the grains in plain light because different amounts of LBE adhered to the different grains. (LBE adhesion is a characteristic sign of corrosion damage.) Figure 26 shows the test pieces of Fe and Cr following the test. There was very minimal corrosion visible on the Cr, which was expected to oxidize more easily than Fe.

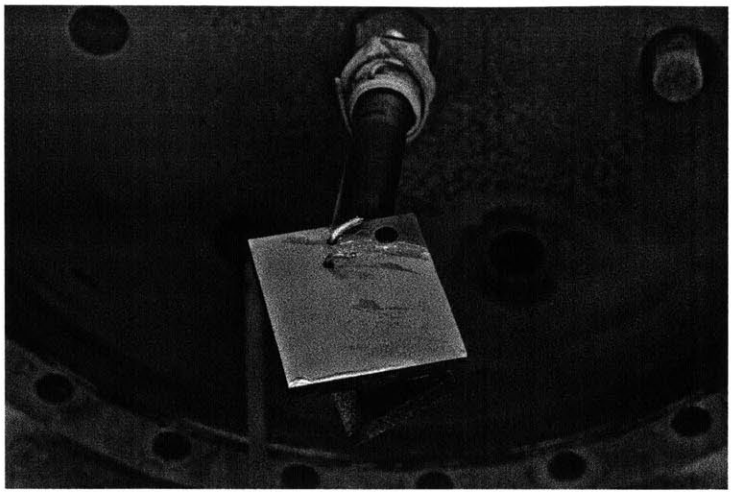

FIGURE 24. The F91 sample, after 30 hours of LBE exposure in a pure H_2 environment at 715°C. Note that the vapor film on the inside of the lid is a grayish-blue color, instead of the yellowish film observed after the second test run, indicating that oxygen contamination was not an issue in this experiment.

These test pieces - in addition to the shiny, oxidation-free surface of the LBE - indicated that the furnace conditions were successfully kept free of significant oxygen contamination during the test.

The F91 and Fe-12Cr-2Si samples from this third test run were used in the subsequent analysis.

5. Results of the Exposure Test

5.1. **Scanning electron microscopy.** Initial pictures were taken at the polished sample face for both Fe-12Cr-2Si (Figures 29 and 30) and the F91 (Figures 31 and 32).

Figure 29 shows Fe-12Cr-2Si at 230x magnification. Some corrosion damage is evident, although it is more obvious at higher magnifications. The damage is not as extensive as that sustained by F91. Interestingly, the attack channels seem to be propagating parallel to the surface, rather than orthogonal to the interface.

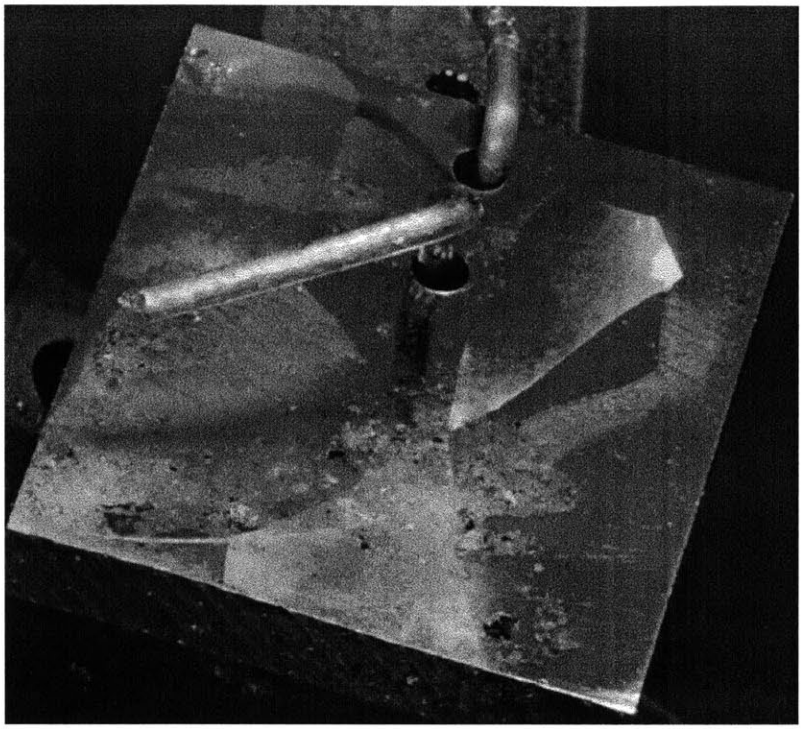

FIGURE 25. The Fe-12Cr-2Si sample, following the 30 hour LBE exposure test in pure H_2 at 715°C. Note that the large grains characteristic of this alloy are clearly visible in plain light - not true of the pre-exposure, polished sample - indicating the possibility that preferential corrosion may have occurred based on grain orientation.

In Figure 30, Fe-12Cr-2Si is shown at 700x magnification. Here, it is possible to see what looks like the first stages of LBE attack. EDX analysis was used to confirm that lead-bismuth eutectic had adhered to the sample. This test suggests that it would be worthwhile to perform longer exposures of Fe-12Cr-2Si in this particular environment to see how corrosion developed in the alloy, since in all other exposure tests, the quick formation of a protective passive film prevented the surface of Fe-12Cr-2Si from corrosion damage.

Figure 31 shows the surface of alloy F91 at 500x magnification. Signs of LBE attack are visible. F91 exhibits fairly uniform corrosion damage across its surface,

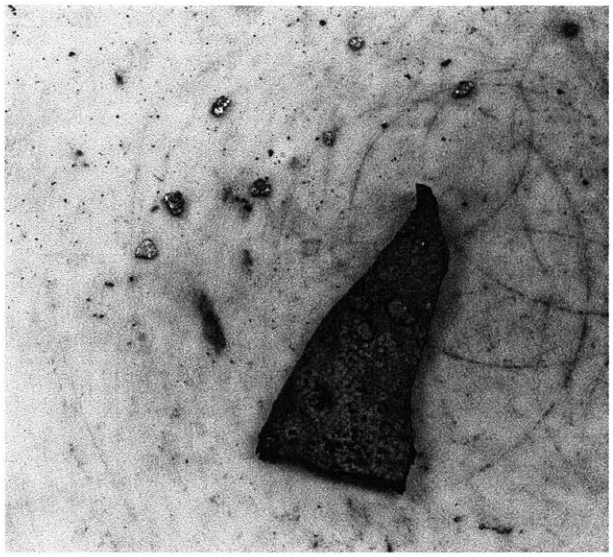

FIGURE 26. The Fe and Cr test pieces showed very minimal oxidation, indicating that the furnace were successfully kept free of significant oxygen contamination. The surface of the LBE was also shiny and silvery in color, and lacked the thick black oxide layer or the gold lead oxide layer of test runs one and two.

with attack channels propagating vertically into the bulk of the metal. A layer of LBE adhered to the corroded surface.

A second view of LBE attack in the F91, at 850x magnification, is given in Figure 32. LBE adhered to the corroded surface, across the entire interface. In Fe-12Cr-2Si, LBE residue was found only inside isolated channels.

5.2. **EDX: Fe-12Cr-2Si.** Figure 33 shows the sample interface at 2000x magnification. This is the section of the Fe-12Cr-2Si sample over which EDX analysis was performed. There has been attack; EDX allowed the confirmation that LBE is inside the attacked zones.

Figure 34 shows the same area, with scans performed for oxygen, chromium, iron, lead, and bismuth. A silicon scan was not performed because the low content of silicon in the alloy would have necessitated a much longer counting time for good

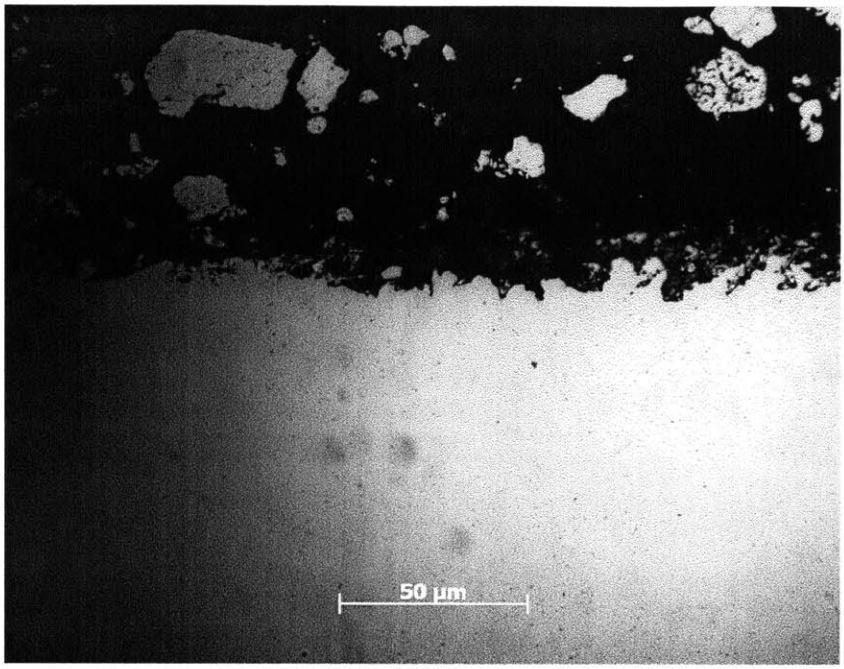

FIGURE 27. **(Optical Microscopy: F91)** The F91 sample was cut, mounted, and polished following 30 hours of exposure to 715°C LBE in an atmosphere of pure H_2. The picture above was taken at 500 times magnification. The black/gray grain structure above the sample is the polished surface of the bakelite/copper mixture used to mount the cut samples. Note that significant corrosion damage is evident.

results, and there was also a high silicon content in the Bakelite, whose detection would not have been particularly informative. Fe and Cr are visible in the sample (pink and dark blue); Pb and Bi are indeed inside the small crevasses where LBE attack occurred at the sample interface, and are visible as the bright blue/lime regions. Note that this is not a result we have obtained before for Fe-12Cr-2Si. Note that there also appears to be slight Cr enrichment at the interface.

Figure 35 shows the same area, with a scan performed only for oxygen. Note that there appears to be slight enrichment at the edge of the interface: due to the highly reducing environment of pure hydrogen, oxygen content inside the experiment was very minimal, but it is possible that these are the beginnings of an oxide layer.

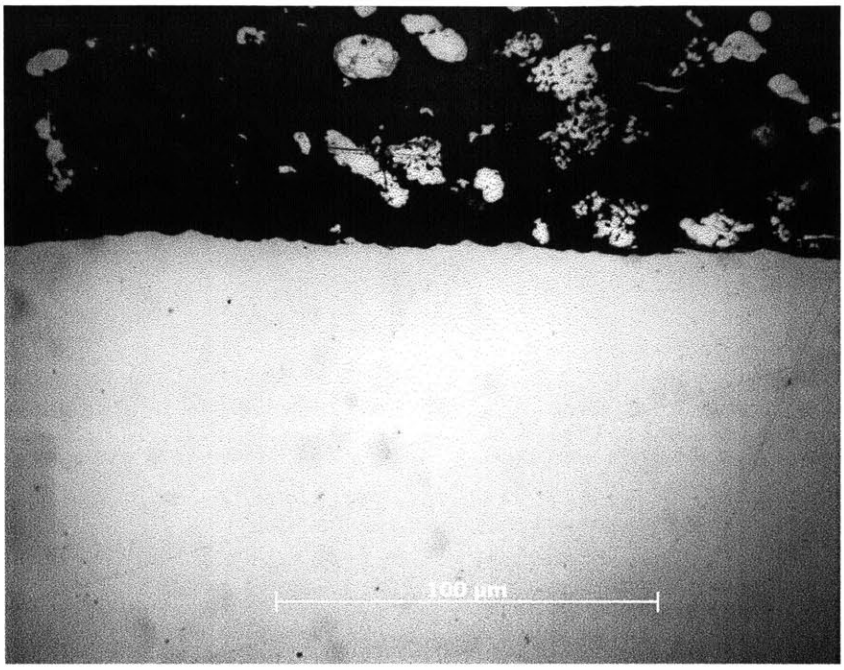

FIGURE 28. **(Optical Microscopy: Fe-12Cr-2Si)** The Fe-12Cr-2Si sample was cut, mounted, and polished following 30 hours of exposure to 715°C LBE in an atmosphere of pure H_2. The picture above was taken at 500 times magnification. The black/gray grain structure above the sample is merely the polished surface of the bakelite/copper mixture used to mount the cut samples. Note that significantly less corrosion damage is observed on the surface in comparison to the sample shown in Figure 27, as expected from previous static LBE corrosion studies using these materials.

5.3. **EDX: F91.** Figure 36 shows the section of the F91 interface that was analyzed via EDX for elemental concentrations. This is taken at 2000x magnification. The interface is corroded, with a layer of LBE on its surface.

Figure 37 shows concentrations of Fe, Cr, Pb, and Bi at the F91 interface. There is clearly a significant amount of LBE that has remained on the surface of the sample, which is characteristic of LBE corrosion attack in this metal. Cr (dark blue) appears depleted at the interface; this is confirmed in Figure 38.

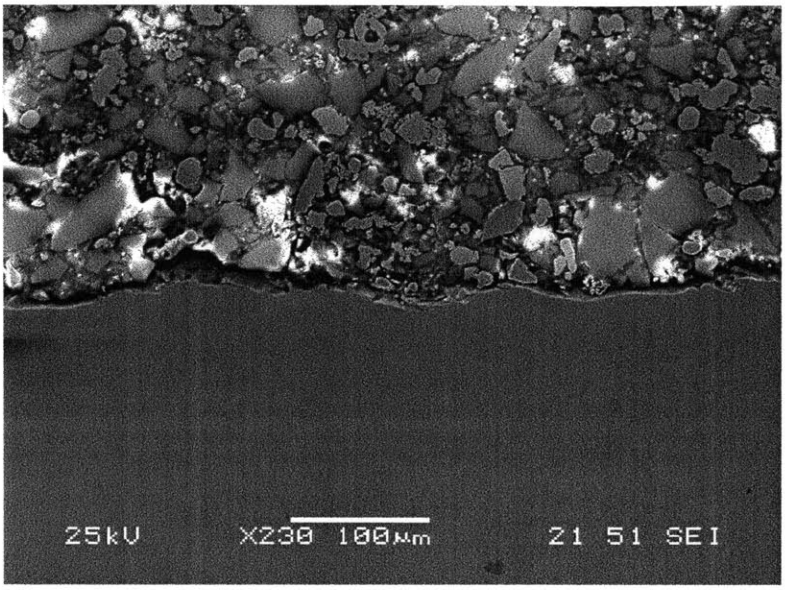

FIGURE 29. **(SEM: Fe-12Cr-2Si)** Fe-12Cr-2Si is shown at 230x magnification. Some corrosion damage is evident, although it is more obvious at higher magnifications. The damage is not as extensive as that sustained by F91. The attack channels seem to be propagating parallel to the surface, rather than orthogonal to the interface.

Figure 38 shows concentrations of Cr and Fe at the interface, and evidences that Cr depletion in the F91 has occurred. Note that it appears that significant Cr depletion has occurred at the sample interface. The depleted Cr (yellow in this image) has migrated through the LBE, leaving an area enriched in iron at the interface. This sort of Cr depletion behavior makes the F91 particularly vulnerable to attack - thus the need for a composite-metal solution of the type proposed in previous studies.

Figure 39 shows counts-per-second/eV versus eV for various elements during the EDX scan of the F91 interface. All expected elements were observed. The high spikes at expected energy levels for Si and Cu were due to the mounting Bakelite, which has high concentrations of both. No unexpected elements were present in significant amounts.

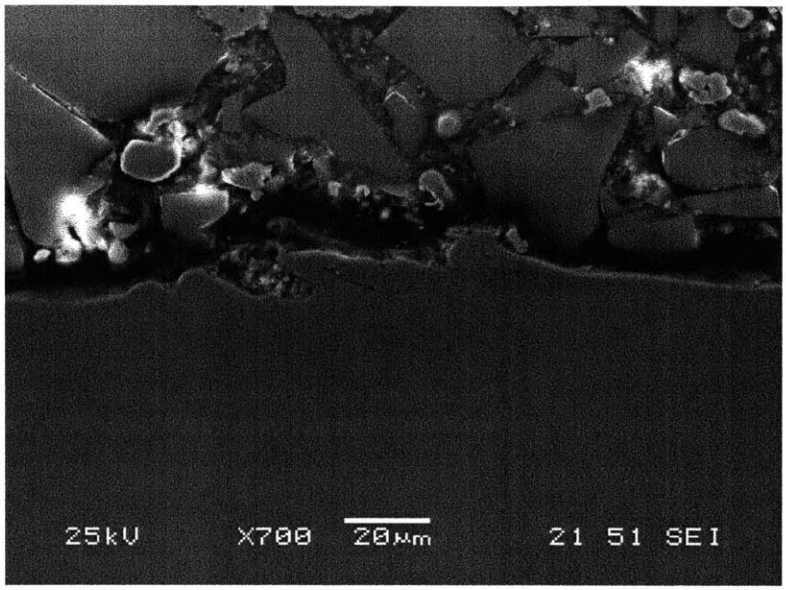

FIGURE 30. **(SEM: Fe-12Cr-2Si)** Fe-12Cr-2Si is shown at 700x magnification. Here, it is possible to see what looks like the first stages of LBE attack. EDX analysis was used to confirm that lead-bismuth eutectic had adhered to the sample. This test suggests that it would be worthwhile to perform longer exposures of Fe-12Cr-2Si in this particular environment to see how corrosion developed in the alloy, since in all other exposure tests, the quick formation of a protective passive film prevented the surface of Fe-12Cr-2Si from corrosion damage.

5.4. **Post-etching Microscopy Results.** Figure 40 shows the stained sample of F91 at 200x magnification. This displays the expected grain structure of F91, which is a ferritic/martensitic steel that was initially quenched and tempered when it was forged. The corrosion attack due to LBE exposure is visible along the top. Note the paler coloring of the sample along the interface, which may be indicative of either the presence of pure ferrite or of edge effects (in which the staining solution is able to permeate the space between the sample and the Bakelite mount, and reacts preferentially with the inside edge of the metal, resulting in a small area near the interface that is stained less than the rest of the sample.) In order to determine the cause of the staining disparity, a line hardness test was performed

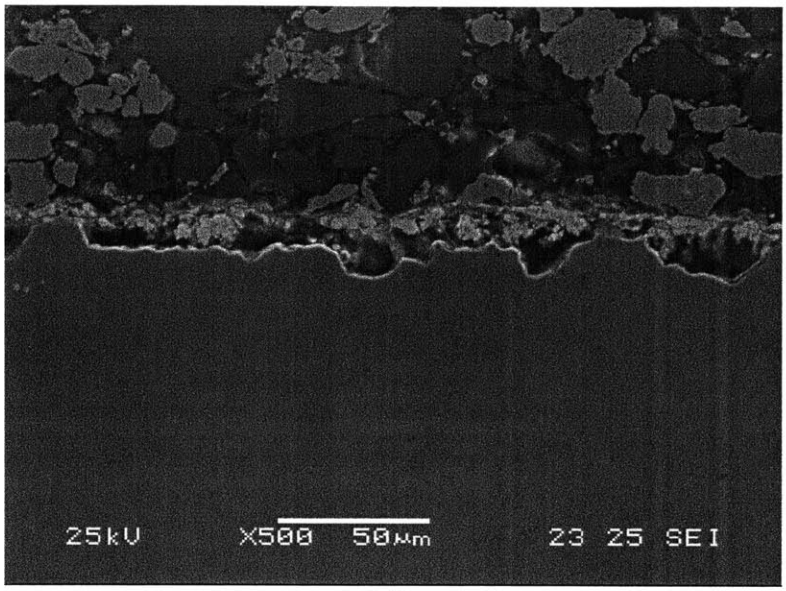

FIGURE 31. **(SEM: F91)** The surface of alloy F91 at 500x magnification. Signs of LBE attack are visible. F91 exhibits fairly uniform corrosion damage across its surface, with attack channels propagating vertically into the bulk of the metal. A layer of LBE adhered to the corroded surface.

on a Leco LM247 microhardness tester using a Vickers tip and 10 grams of force with a 15 second dwell time per point.

If the lighter area was indeed ferrite, it was expected that it would be significantly less hard than the more darkly stained areas. However, no significant difference between the hardness of the darkly stained areas and the lightly stained edge was found, and so it was assumed that the color discrepancy was merely an edge effect.

For the Fe-12Cr-2Si sample, deep etching along the grain boundaries was observed, as was expected of this etchant. Several crack-like features were apparent within grains that were not observed prior to etching; these are visible in the 100x magnification images of the sample interface (Figure 41) and of the boundary intersection of three distinct grains. Diamond-shaped pits are visible throughout the sample following etching: Figure 43 shows that their orientation is grain-dependent,

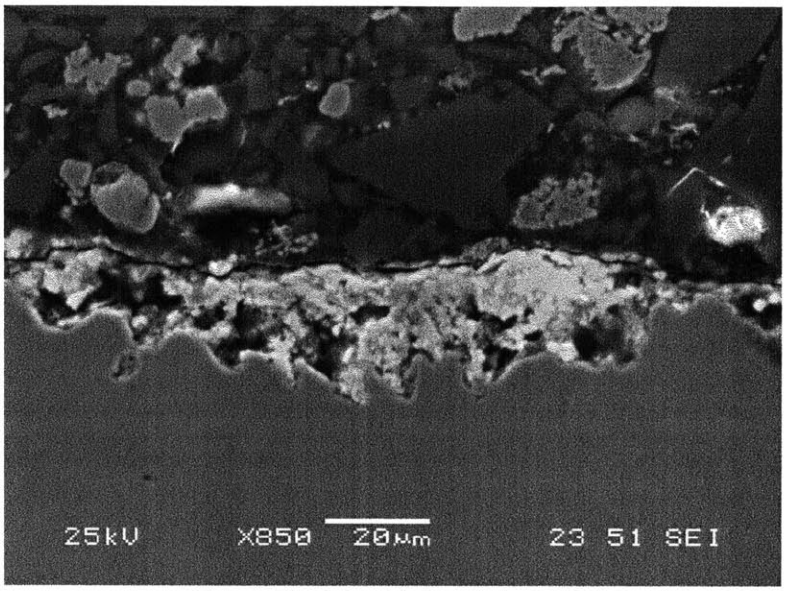

FIGURE 32. **(SEM: F91)** A second view of LBE attack in the F91, at 850x magnification. LBE adhered to the corroded surface, across the entire interface. In Fe-12Cr-2Si, LBE residue was found only inside isolated channels.

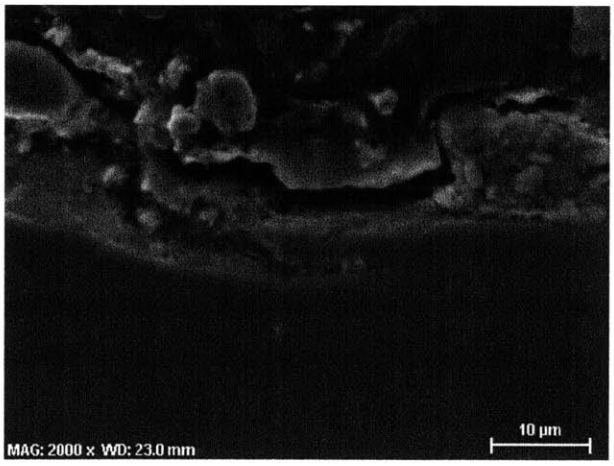

FIGURE 33. **(EDX: Fe-12Cr-2Si)** The section of the Fe-12Cr-2Si sample over which EDX analysis was performed. There has been LBE attack; EDX allowed the confirmation that LBE was inside the attacked zones.

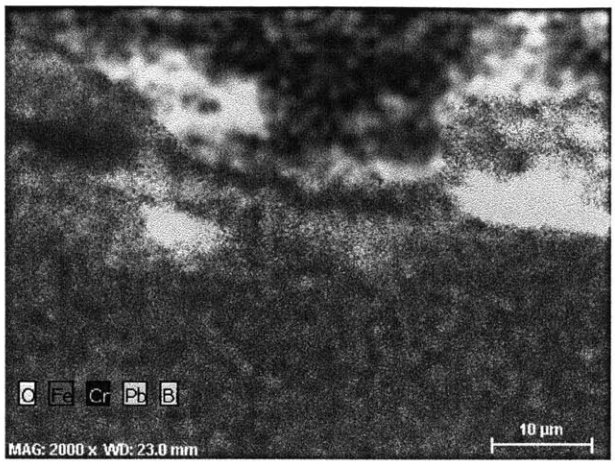

FIGURE 34. **(EDX: Fe-12Cr-2Si)** A scan of all the relevant elements in this sample. Fe and Cr are visible in the sample (pink and dark blue); Pb and Bi are indeed inside the small crevices where LBE attack occurred at the sample interface, and are visible as the bright blue/lime regions. Note that this is not a result that has been obtained before for Fe-12Cr-2Si. Note that there also appears to be slight Cr enrichment at the interface.

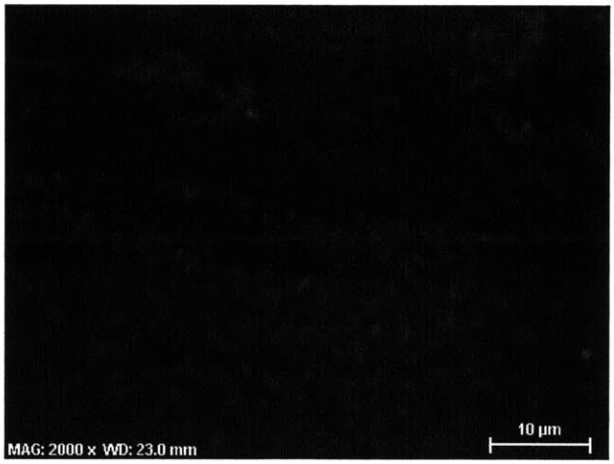

FIGURE 35. **(EDX: Fe-12Cr-2Si)** Oxygen EDX map of the Fe-12Cr-2Si sample. Note that there appears to be slight enrichment at the edge of the interface: due to the highly reducing environment of pure hydrogen, oxygen content inside the experiment was very minimal, but it is possible that these are the beginnings of an oxide layer.

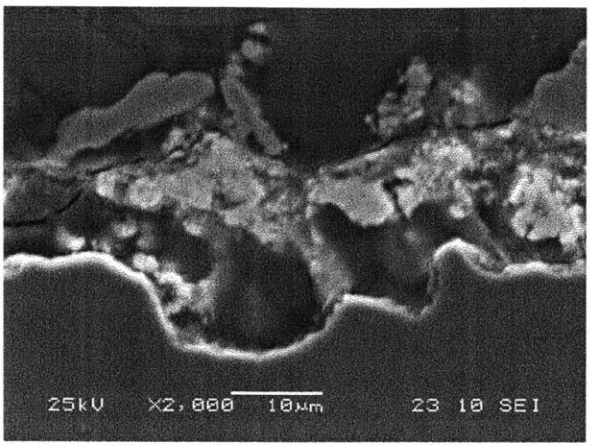

FIGURE 36. **(EDX: F91)** SEM image of F91 taken at 2000x magnification. This area of the F91 was scanned for elemental concentrations via EDX. The interface is corroded, with a layer of LBE on its surface.

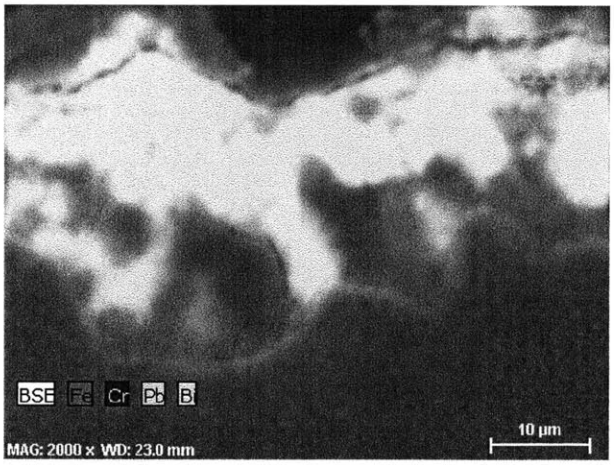

FIGURE 37. **(EDX: F91)** This scan of the F91 interface shows concentrations of Fe and Cr, as well as Pb and Bi. There is a significant amount of LBE that has remained on the surface of the sample, which is characteristic of LBE corrosion attack in this metal. Cr (dark blue) appears depleted at the interface.

suggesting that they are crystallographic etch pits. Previous work suggests that these etch pits form at dislocations cores inside each grain.

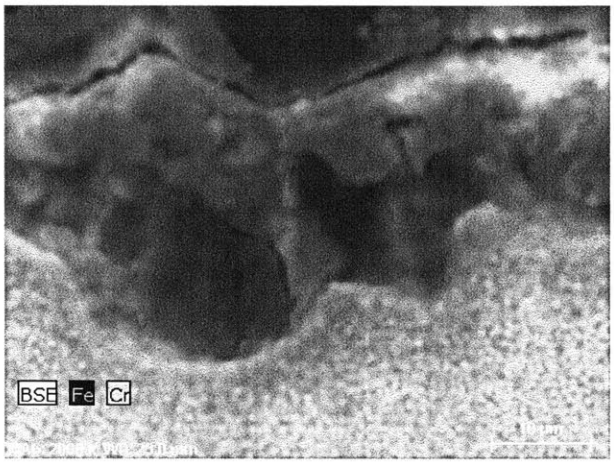

FIGURE 38. **(EDX: F91)** This scan - performed on the same area of the F91 interface as in Figures 36 and 37 - was performed to show concentrations of Fe and Cr. Note that significant Cr depletion has occurred at the sample interface. The depleted Cr (yellow in this image) has migrated through the LBE, leaving an area enriched in iron at the interface. This sort of Cr depletion behavior makes the F91 particularly vulnerable to attack - thus the need for a composite-metal solution of the type proposed in previous studies.

6. ANALYSIS

The purpose of this study was to simulate crevice corrosion in the alloys of interest by immersing them in LBE at reactor operating temperature in a highly reducing environment, achieved by running a pure H_2 flow through the system.

F91 showed signs of LBE attack along the material/environment interface: this is visible in Figures 27 and 40. The attack channels were approximately 10 μm deep for this 30 hour exposure test. Figure 37 shows that lead-bismuth residue remained in the attack channels and along the surface. This was observed as well in the F91 exposed to LBE at these temperatures in previous studies [3]. Metal adheres to oxide-free metal: the presence of the LBE in the attack channel and along the surface of the F91 indicates that no oxide layer was formed. This was as expected: F91 does not tend to form sufficiently protective oxide layers under

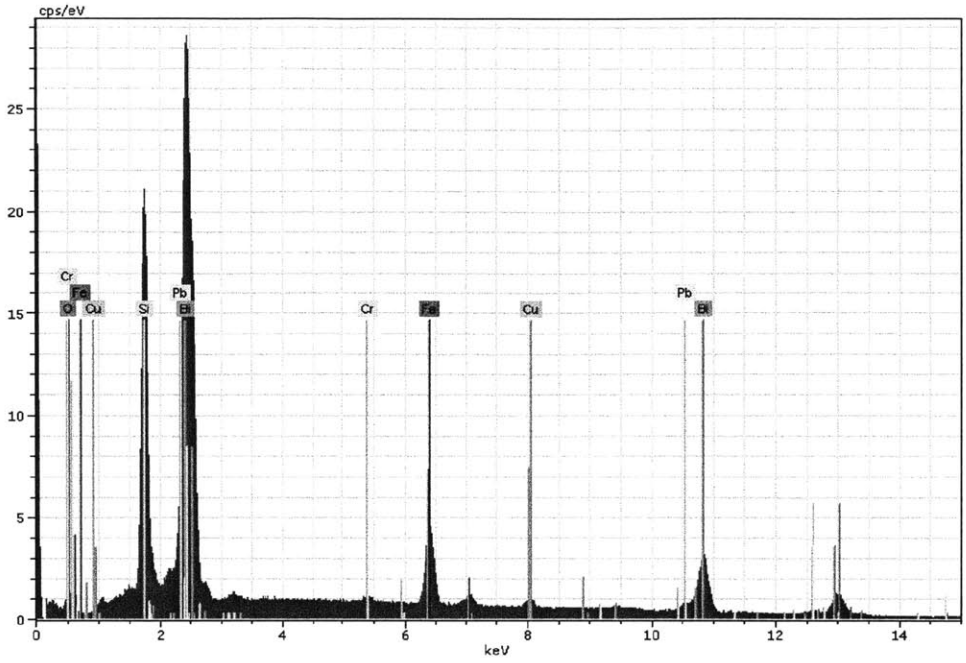

FIGURE 39. **(EDX: F91).** EDX spectrum of Pb, Bi, Fe, and Cr in alloy F91 at the material/fluid interface. No unexpected elements were observed. The high spikes at expected energy levels for Si and Cu are due to the composition of the Bakelite used to mount the samples.

these conditions, and as a result, it is highly susceptible to LBE corrosion. This was, of course, the motivation for weld-overlaying Fe-12Cr-2Si over F91 in the first place.

Figure 38 shows that chromium was depleted at the surface of F91. An excess of chromium can be seen at the outer edge of the LBE residue layer, indicating the chromium migrated through the LBE and left the metal interface enriched in iron. Even in a less reducing environment, this behavior made it difficult for F91 to form a protective oxide layer. Chromium is especially effective at increasing the corrosion resistance of a metal, since it forms protective chromium oxides **??**. However, in high temperature LBE - even at higher oxygen potentials - chromium oxides cannot form at the F91 surface and prevent further attack because the

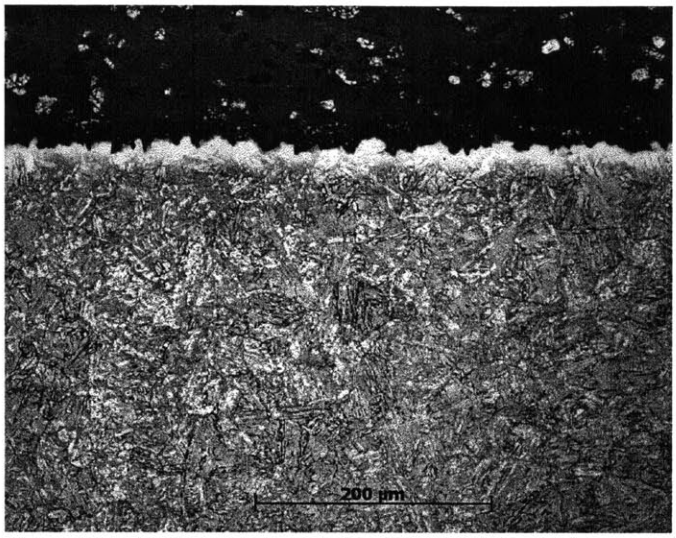

FIGURE 40. **(Optical Microscopy: F91, post-stain)** The stained F91 sample is shown at 200x magnification. It displays the ferritic/martensitic grain structure expected of this steel, and the areas of corrosion attack are visible at the interface. The lightness along the edge was found to be an edge effect that occurred during the staining process, and it is not indicative of a microstructural change at the sample's surface.

chromium is so quickly depleted: note that this exposure test was for only thirty hours.

The results for Fe-12Cr-2Si were more surprising. What appeared to be slight corrosion was observed during optical microscopy (Figure 28), although the areas of attack were significantly smaller and shallower than those observed in F91. (For comparison, Figure 27 shows F91 at the same level of magnification, and the amount of damage sustained by this metal is greater.) However, in previous experiments, Fe-12Cr-2Si showed practically no corrosion damage at all. The SEM/EDX analysis was particularly useful for gaining further insight into the damage on this alloy, in order to confirm that corrosion damage had cocurred. Figure 33 shows the interface at 2000x magnification: it seems possible that the interface shows signs of corrosion damage, although this image alone is not conclusive. However, EDX results shown

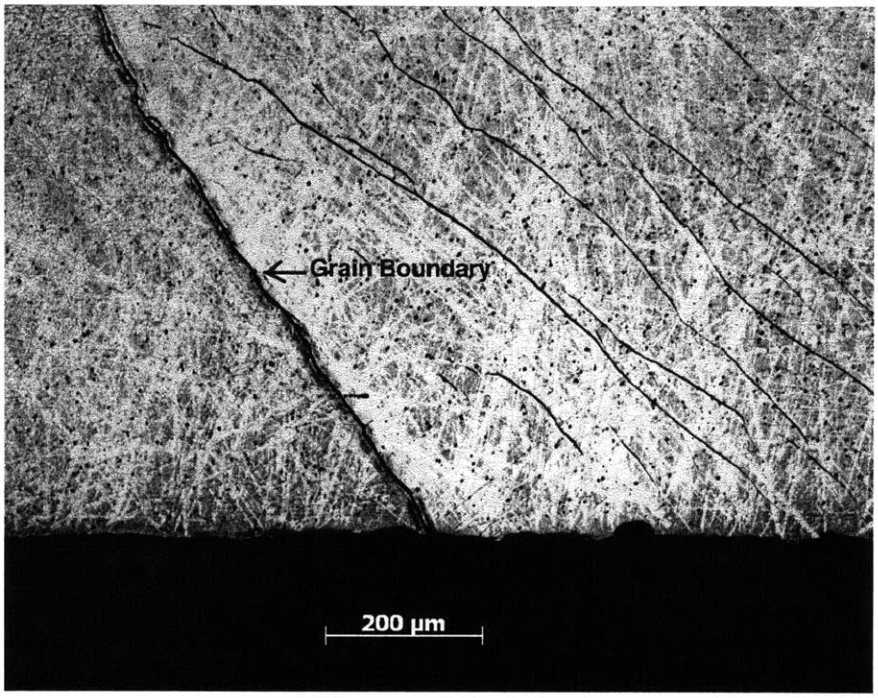

FIGURE 41. **(Optical Microscopy: Fe-12Cr-2Si, post-etch)** Etching has revealed dislocations in the Fe-12Cr-2Si alloy. Dislocation cores that run perpendicular to the photographed surface appear during etching as point-like pits; dislocation cores that run parallel to the photographed surface appear as diagonal, crack-like lines (seen in the grain on the right-hand side). As the sample is etched for longer periods of time, more of the parallel-to-surface dislocation cores become visible. The bends and kinks in the parallel-to-surface dislocation cores are likely caused by defects in the alloy lattice that have impeded movement of the dislocation.

in Figure 34 confirm that LBE attack did, in fact occur: lead and bismuth are present inside two distinct areas of attack. The Fe-12Cr-2Si displayed much better corrosion resistance than did F91, as expected; the attack channels were fewer, shallower, and there was no distinct layer of LBE across the interface. However, it was significant that there was visible corrosion with LBE inside: this behavior was not observed in previous tests. The presence of LBE indicates, again, that oxide

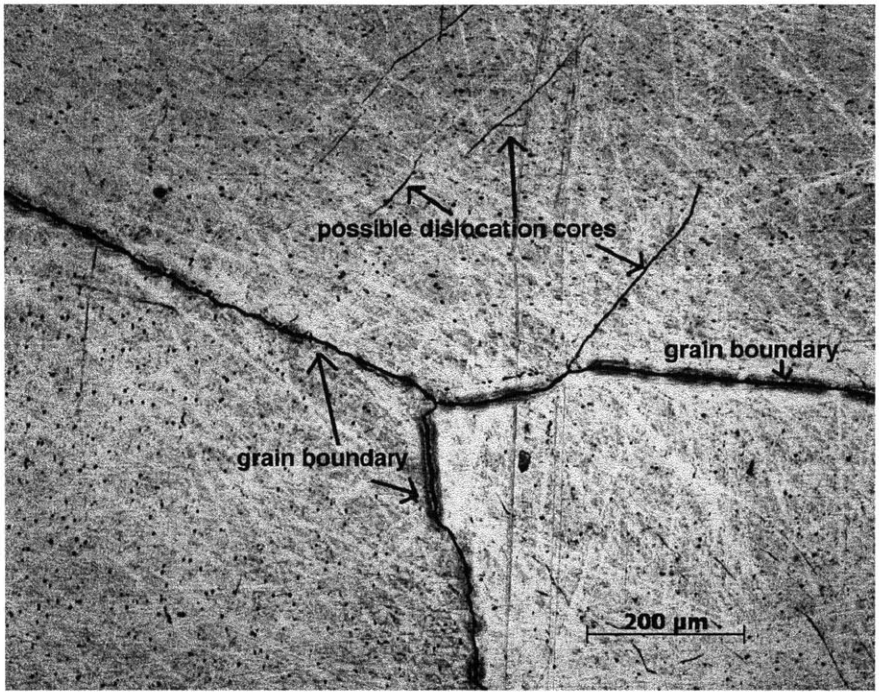

FIGURE 42. **(Optical Microscopy: Fe-12Cr-2Si, post-etch)** The image shows a point in the Fe-12Cr-2Si alloy where three grains meet. Etch pits are visible as small black dots; the features in the top grain that look like cracks may possibly be dislocation cores that are parallel to the surface.

layers did not fully form: LBE cannot adhere to an oxide layer, but it will adhere to a bare metal interface.

Figure 35 shows an oxygen scan performed along the interface. Comparison of Figures 33 and 34 shows what may actually be a slight enrichment of oxygen at the surface of the metal. A longer count time would be needed to conclude this definitively. Fe-12Cr-2Si is such a desirable alloy for overlay on F91 because it forms protective passivating oxide layers so quickly, so it was expected that some oxide formation would be observed here as well. However, the environment inside the exposure experiment was kept purposely reducing: oxygen content inside the furnace was reduced to negligible levels at the start of the test, and pure H_2 gas

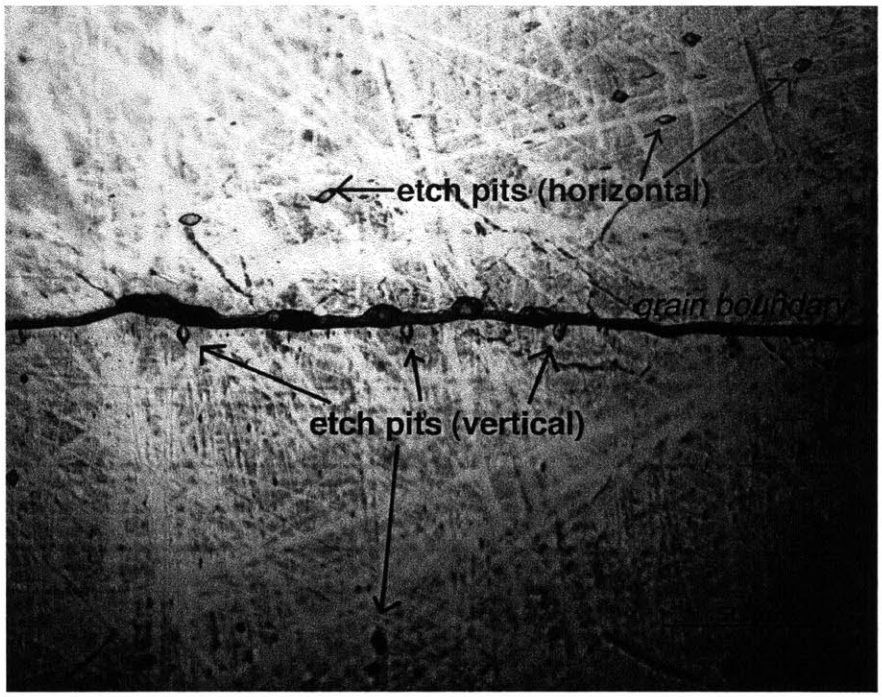

FIGURE 43. **(Optical Microscopy: Fe-12Cr-2Si, post-etch)** This image was captured at 500x magnification along a grain boundary in order to show the orientation of the etch pits. In the top grain, they are oriented in the horizontal direction; in the bottom grain, they are oriented in the horizontal direction. This, combined with their characteristic diamond shapes, indicates that they are crystallographic etch pits. Their orientation is determined by the orientation of the crystal lattice within a grain.

was used. If a mixture of H_2 and oxygen gas had been used, it would have been expected that the distinct formation of oxide layers would be observed, and that the corrosion resistance displayed would have been much higher.

Figure 43 shows a closeup of the crystallographic etch pits observed on the Fe-12Cr-2Si sample following sixty seconds of etching with the hydrofluoric acid mixture. These can also be observed as small black dots in Figures 41 and 42. During initial metallography at low magnification, it was postulated that these might be etch pits. Figure 43 confirms that this is so. Etch pits display a distinct diamond

shaped structure that share a common orientation within each grain; they are not randomly rotated within a grain. Different grains, however, may display different orientations, since the crystal lattices of each grain may be rotated relative to each other. In this figure, the etch pits are oriented horizontally in the top grain, and vertically in the bottom grain (for the bottom grain, the etch pits closest to the etched grain boundary display this the most clearly). Etch pits are believed to occur at the sites of dislocations in the sample. Figure 41 shows both pits and kinked structures: it is likely that the 'cracks' are also etch pits that form along laterally oriented dislocation cores. In this case, the cores run parallel to the surface of interest; the etching revealed these. Dislocation cores that ran perpendicular to the surface of interest are revealed as the point-like etch pits. As etching is extended, one would expect more of the parallel-to-surface dislocation cores to be revealed. These dislocations are expected to have formed during the fabrication of the samples.

7. Conclusions and Future Work

Ultimately, the purpose of this experiment was twofold. The first was to adapt the experimental setup for the high-temperature LBE exposure of Fe-12Cr-2Si and F91 for the simulation of crevice corrosion. The second goal was to use the adapted setup to investigate whether or not crevice corrosion was likely to be an important concern in LBE applications that use the F91/Fe-12Cr-2Si composite metal.

7.1. Experimental Considerations. The following list outlines the most important lessons learned from conducting this experiment with pure hydrogen gas to simulate crevice corrosion.

- The preparation of the furnace (backfilling with argon gas, baking out at high temperature, securing the lid with the correct amounts of torque, and checking

for gas leaks) are especially important when using pure H_2 gas, since it is necessary to minimize the oxygen content inside the furnace as much as possible in order to simulate the highly reducing environment inside a crevice.

- Due to safety regulations, it is not possible to have more than one canister of hydrogen at a time. Since the hydrogen ran out so quickly, it may be necessary to adapt the experimental setup in order to perform longer exposure tests. The best way to do this might be to develop a procedure whereby it was possible to quickly change out hydrogen canisters without contaminating the internal environment of the furnace. Another option, which is likely more feasible in the short term, would be to minimize the length of the stainless steel tubing that connects the hydrogen canister to the furnace, which would simply require rearrangement of the experimental setup and reworking the existing stainless steel connections. It will also be useful to obtain a quantitative model of hydrogen diffusion rates out of this system.
- Following the second test, a yellowish film on the inner lid of the furnace and a gold film on the surface of the resolidified LBE indicated moderate oxygen contamination. Black films indicated severe oxygen contamination. A successful test in such a reducing environment will show a shiny, silvery surface on the resolidified LBE, a gray film on the inner lid surface, no visible corrosion on the iron test pieces, and only very slight oxidation (a moderate, bluish-gray coating) on the chromium test piece.
- In order to prevent edge effects in the staining of F91 with Kaling's reagent, a different mounting material might be better. The advantage of the copper suspension is that it is more efficacious for SEM work due to its high conductivity.

- Ideally, F91 and Fe-12Cr-2Si should be polished separately following the exposure test and the subsequent cutting and mounting of the samples. To save time, the four samples were polished together. However, it is difficult to prevent carbides from being pulled out of the F91 and scratching the Fe-12Cr-2Si interface when they are polished together. Separate polishing is advised in order to obtain better micrographs of Fe-12Cr-2Si with less surface scratching.
- Researchers using this setup should be aware of temperature discrepancies: the temperature read by the thermocouple in the furnace coil (corresponding to the set point temperature on the furnace controls) is not the same as the thermocouple reading inside the furnace, which is not the same as the thermocouple reading inside the molten LBE. It is possible to get accurate temperatures, of course, but future experimenters should take note of this particular aspect of this experimental setup.

7.2. **Exposure Test Results.** The key result of this experiment was that Fe-12Cr-2Si has been shown to be vulnerable to corrosion attack in purely reducing environments, which may occur in crevices/occluded regions at the surface of a metal exposed to a flowing working fluid.

As expected from previous experiments, F91 exhibited corrosion damage after thirty hours of exposure to LBE at 715°C in a highly reducing environment. LBE remained adhered to the metal, indicating that protective oxide layers did not form. Figure 38 suggests that this is due to chromium depletion from the F91 alloy at the interface. This behavior is expected of F91. In the composite system of F91/Fe-12Cr-2Si, this is not problematic in any environment with sufficient oxygen potential for oxide formation in Fe-12Cr-2Si. Once the passivating layer has formed - a process that occurs very quickly, even in the most reducing environments -

the Fe-12Cr-2Si is resistant to metal attack, and provides a barrier between the vulnerable F91 and the high-temperature LBE.

However, Fe-12Cr-2Si also exhibited slight corrosion damage after thirty hours of exposure, as evidenced by the small corrosion attack channels observed along the surface. LBE adherence in these channels - confirmed by EDX analysis - shows that the protective oxide layer usually associated with this metal did not fully develop, most likely due to the extremely low oxygen content inside the experimental setup. Fe-12Cr-2Si, therefore, appears to lose its protective abilities under extremely reducing conditions.[12]

Fe-12Cr-2Si is overlaid on top of F91 in the composite metal of interest in order to provide excellent corrosion resistance. However, the fact that Fe-12Cr-2Si did display corrosion damage after this thirty hour corrosion test suggests crevice corrosion could be a significant damaging mechanism in an operating LBE-cooled reactor using this composite as a structural material, especially over extended periods of time. Corrosion of Fe-12Cr-2Si itself is not the problematic issue here because Fe-12Cr-2Si does not provide structural support to the piping or the cladding. However, if crevice corrosion was to be initiated in an occluded region or surface defect at the Fe-12Cr-2Si layer, and was to then propagate deeply enough to breach that layer, the F91 would then be vulnerable to attack. F91 corrodes severely and quickly in LBE heated to reactor operating temperatures. This is the major concern, since F91 provides the structural support to the cladding and coolant piping, allowing it to withstand the mechanical and thermal stresses of the aggressive fast reactor environment. Therefore, it is imperative to ensure that the fabrication processes

[12]Note that Fe-12Cr-2Si and F91 have similar levels of chromium. In F91, chromium is depleted due to dissolution. The major difference is the silicon content of Fe-12Cr-2Si: this seems to be the reason why dissolution is not as much of a problem in the Fe-12Cr-2Si. One reason that longer tests are desired in the future will be to see what happens in Fe-12Cr-2Si when chromium dissolution is more important, and a silicon-rich layer is formed.

- from the weld-overlay of Fe-12Cr-2Si to the extrusion of piping and cladding - do not yield surface defects that could become initiation sites for crevice corrosion during reactor operation.

7.3. **Future Work.** In the future, it would be useful to perform several longer corrosion tests under these experimental conditions in order to obtain more data. In particular, it would be very interesting to gain a deeper understanding of how Fe-12Cr-2Si sustains corrosion damage in a purely reducing environment. It would also be useful to perform LBE exposure tests of Fe-12Cr-2Si in varying environments in order to determine the minimum oxygen levels required for effective protection from passivating oxide layers that form on the surface of this alloy. Also, in order to determine if a small oxide layer did form on the Fe-12Cr-2Si under these conditions, one of the two Fe-12Cr-2Si samples from this test were sent to Finland for very high resolution microscopy (100,000 x). It will be interesting to see these results and incorporate them into future papers.

It would also be interesting to consider some sort of 'pre-passivation' process to incorporate into the fabrication of F91/Fe-12Cr-2Si fuel cladding and coolant piping. Perhaps it would be possible to ensure that a passivating layer is fully developed over the entire surface area composed of Fe-12Cr-2Si as part of the composite fabrication process. It may be necessary to electropolish components in order to eliminate surface asperities.

Finally, since it is now expected that Fe-12Cr-2Si could sustain some corrosion damage inside a crevice in the surface of the metal, it would be valuable to study the Fe-12Cr-2Si/F91 composite for signs of crevices, or crevice formation following exposure to LBE. This would allow determination of the possibility that crevice corrosion might become a significant concern in an LBE-cooled reactor, and perhaps to investigate ways in which to ensure that crevice formation is minimized.

8. Acknowledgements

First, to Dr. Mike Short: working on the Functionally Graded Composite for LBE Cooled Reactors project at the Uhlig Corrosion lab during the past two and half years has been the most valuable part of my experience so far at MIT. (Great success!) Even more so than rowing, more so than living with my beloved Burton Third Bombers, more so than the Shakespeare Ensemble, and maybe even more than the lunch buffet at Desi Dhaba. Whether we're plastering the lab with **Danger!** signs or sneaking through fish markets of Tokyo at 5 AM, we always seem to have memorable adventures. More thanks are of course due to Professor Ballinger for his continued support and mentorship of UROP students in the Uhlig lab: I am so grateful for all of the opportunities you have provided to me. I would also like to acknowledge the U.S. Department of Energy and the NERI project for their financial support of the earlier stages of this project, which has taught me so much over the past three years. Thank you to Port-a-Party and to the torque wrench from the tool box in the lab across from the polishing room: Mike and I couldn't have done it without you. More thanks to Mike (again), Tim, Jon, and Marina: who would have guessed that the company, guidance, and practical joking (on and of) three cynical (and one not-so-cynical) grad students would be the highlight of my undergrad career? By the time this undergraduate thesis is handed in, all four of you will have officially finished your Ph.D work. I love you all. No, really. Even you, Tim, even though you purport to like dumb Lauren better than me. Last but not least, to Heather Barry, for having become some odd combination of academic administrator, older sister, and best friend over the past four years. Thank you for making Room 24-102 and the NSE Department - otherwise known as the Society for the Preservation of Precious Bodily Fluids - feel so much like home. I could not

imagine getting through these past four years without the the unerring support of you and Clare. Love.

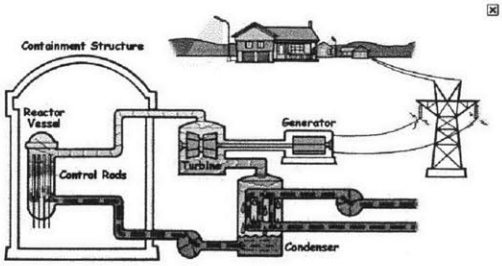

FIGURE 44. This is not relevant.

REFERENCES

[1] U.S. DOE Nuclear Energy Research Advisory Committee and the Generation IV International Forum. A technology roadmap for generation iv nuclear energy systems. Technical report, U.S. Department of Energy, 2002.

[2] *Proceedings of the Workshop on Utilisation and Reliability of High Power Proton Accelerators*, Mito, Japan, October 1998. pp. 155-156.

[3] M. P. Short. *The Design of a Functionally Graded Composite for Service in High Temperature Lead and Lead-Bismuth Cooled Nuclear Reactors.* PhD thesis, MIT, 2010.

[4] Philippe Marcus, ed. *Corrosion Mechanisms in Theory and Practice: Second Edition*, Marcel Dekker, Inc., New York, 2002.

[5] Tomohiro Furukawa, Georg Müller, Gustav Schumacher, Alfons Weisenburger, Annette Heinzel, Frank Zimmermann, and Kazumi Aoto. Corrosion behavior of FBR candidate materials in stagnant Pb-Bi at elevated temperature. *Journal of Nuclear Science and Technology*, 41(3):6, 2004.

[6] R.L. Klueh and A.T. Nelson. Ferritic/martensitic steels for next-generation reactors. *Journal of Nuclear Materials*, 371(1-3):3752, September 2007.

[7] J. Robertson and M. Manning. Healing layer formation in Fe-Cr-Si ferritic steels. *Materials Science and Technolgoy*, 5(8), 741-753, 1989.

[8] J. Y. Lim. *Effects of Chromium and Silicon on Corrosion of Iron Alloys in Lead-Bismuth Eutectic.* PhD thesis, MIT, 2006.

[9] H. A. Wriedt and H. Okamoto. Binary alloy phase diagrams. In *ASM Handbooks Online, Volume 3 - Alloy Phase Diagrams*, volume 3. ASM, 2004.

[10] K. Ravindranath and S. N. Malhotra. The influence of aging on the intergranular corrosion of 22 chromium-5 nickel duplex stainless steel. *Corrosion Science*, 37(1):121 - 132, January 1995.

[11] W. C. Leslie. *The Physical Metallurgy of Steels.* Hemisphere Publishing Corp., USA, 1981. ISBN 978-1878907257.

[12] J. N. DuPont, J.R. Regina, and K. Adams. Improving the weldability of FeCrAl weld overlay coatings. *Fossil Energy Materials Conference*, 131-137, 2007.

[13] M. K. Miller, K. F. Russell, J. Kocik, and E. Keilova. Embrittlement of low copper VVER 440 surveillance samples neutron-irradiated to high fluences. *Journal of Nuclear Materials*, 282(1):8388, November 2000.

[14] A. Kryukov, Yu. Nikolaev, and A. Nikolaeva. Composition effects in the radiation embrittlement of low-alloy steel. Atomic Energy, 84(4):304 - 307, April 1998.

[15] Denny A. Jones. *Principles and Prevention of Corrosion.* Prentice Hall, 2nd Edition, 1996.

[16] M. P. Short, S. E. Ferry, S. Morton, R. G. Ballinger. Diffusional stability of ferritic martensitic steel composite for service in advanced lead bismuth cooled nuclear reactors. *International Heat Treatment and Surface Engineering*, 4(2) pp. 74-80 (2010).

[17] S. E. Ferry and M. P. Short. *The Design of a Functionally Graded Composite for Service in a High Temperature Lead and Lead Bismuth Eutectic Cooled Nuclear Reactor.* 3rd International Nuclear Energy Symposium, Tokyo, Japan, 2010.

[18] G. Müller, G. Schumacher, and F. Zimmerman. Investigation on oxygen controlled liquid lead corrosion of surface treated steels. *Journal of Nuclear Materials*, 278(1):85-95, February 2000.

[19] Mohammed Ismail Abdulsalam, 'Behaviour of crevice corrosion in iron.' Corrosion Science **47** (2005) 1336-1351

[20] Ning Li. Active control of oxygen in molten lead-bismuth eutectic systems to prevent steel corrosion and coolant contamination. *Journal of Nuclar Materials* 100(1), 73-81, 2002.

[21] S. Bernhardsson, L. Eriksson, J. Oppelstrup, I. Puigdomenech, and T. L. Wallin, 8th International Congress on Metallic Corrosion, Mainz, Germany, 1981, 193-198.

[22] J. W. Oldfield, T. S. Lee, and R. N. Kain, *Corrosion Chemistry in Pits, Crevices, and Cracks*: (A. Turnbull ed.), Her Majesty Stationery Office, London, 1987.

[23] J. W. Oldfield, 19th Journées des Aciers Spéciaux - International ymposium on Stainless Steels, Saint Etienne, France, 1980.

[24] H. S. Khatak and Baldev Raj, Eds. *Corrosion of Austenitic Stainless Steels: Mechanism, Mitigation and Monitoring*, Narosa Publishing, USA, 2002. ISBN 978-1855736139.

[25] B.F. Gromov et al., 'Use of lead-bismuth coolant in nuclear reactors and accelerator-driven systems.' *Nuclear Engineering and Design.* **173**, 1997. 207-217.

[26] Y. Fukai and H. Sugimoto. Diffusion of hydrogen in metals. *Advances in Physics*, 34(2):263-326, 1985.

[27] Gary S. Was. *Fundamentals of Radiation Materials Science: Metals and Alloys*, Springer, New York, 1997. ISBN 978-3540494713.